



School of Photovoltaic and Renewable Energy Engineering

Faculty of Engineering

The University of New South Wales

The underperformance of PV Systems on the DC Side- Understanding shading Effects in PV Systems using LIDAR

By

Rahul Ashwin Mahendhran

Thesis submitted as a requirement for the
Degree of Masters of Engineering Science

Submitted : August, 2024
Supervisor: Dr Fiacre Rougieux

Student ID: Z5353624

Abstract

The growing emphasis on monitoring PV systems and the rapid evolution of diagnostic practices are improving the practical functionality of solar plants and reducing power output variability. In a photovoltaic (PV) solar plant, optical losses are crucial in determining overall energy production and yield across the year. Research has demonstrated the potential of using Geographic Information Systems and LIDAR data to estimate the shadowing effect on rooftop and commercial-scale PV systems over a broader range of areas throughout the year. By modelling geospatial data (LIDAR) along with the sun's path over a specific location, we can effectively determine the amount of time a system is shaded. Accurate estimations and analysis of the shadowing impact of PV panels would improve the annual energy yield assessment of the system and enhance estimation techniques for forecasting the solar PV energy penetration to the grid based on the plant's location and orientation.

The study focuses on analyzing the underperformance PV string due to shading using LIDAR technology. It demonstrates shading performance in a simulated environment and compares it with actual data from a PV system. The study uses the Developmental Impact Analysis Tool from ArcGIS to estimate shading on a 3D model, employs Hillshade Analysis to generate a time series projection of the shading profile of a PV string in the system, and compares the impact on the reduction of DC power to the inverter.

The Shading Factor, modelled from the LIDAR data, shows a close correlation with the shading factor and the actual DC Parameters from the studied PV String. The reduction of the DC Current as a result of the increase in the shading over the PV String was evident, therefore causing a reduced power output from the PV String to the inverter. The effect of the modelled module temperature on the DC voltage from the string was observed.

Successfully estimating the duration and causes of shading would allow for implementing strategies to address shading through optimal placement and orientation and regular trimming or removal of obstacles.

Acknowledgment

I want to acknowledge the tireless efforts and unwavering support of my thesis advisor, Dr. Fiacre Rougiex. His valuable insights and feedback have been instrumental in guiding the motive of this study. I would also like to thank, all the faculties who had helped me gather data for the study. I am grateful for my friends and family's guidance and encouragement throughout this journey.

Lastly, I would like to express my gratitude to all the researchers in the domain whose work and insights have been a great motive and a leading direction for my study and made this research possible.

Contents

List of Figures	vi
List of Tables	viii
List of Abbreviations	ix
1. Introduction	1
2. Background	1
3. Literature Review	2
3.1 Overview of the causes of loss of performance in Photovoltaic Power Plant	2
3.2 Causes of DC Losses in PV Plants.....	3
3.3 Preliminary Study	5
3.3.1 Shadowing Effects on PV	5
3.3.2 Current Estimation Techniques for Shading Losses in PV	5
3.4 LIDAR and GIS Technology	7
3.5 Application of LIDAR and GIS in the Renewable Energy Industry	8
3.6 Estimation of Shading and Annual Yield through LIDAR	9
3.6.1 Digital Terrain Map (DTM)	9
3.6.2 Digital Surface Map (DSM).....	9
3.7 DTM and DSM-Based Shading Models.....	10
3.8 Research Gap	12
3.8.1 Limited Utilization of LiDAR with Performance Models:	12
3.8.2 Underdeveloped Predictive Analytics for Shading Impact:.....	13
3.9 Summary	13
4. Experimental Methods	14
4.2 Identifying Required Data Types and Potential Sources	15
4.3 Site Selection.....	18
4.4 Working with LIDAR	20
4.4.1 Preprocessing LIDAR Data.....	20
4.4.2 Generating Building Footprint.....	21
4.4.3 Generating 3D Building Multipatch:.....	21
4.4.4 Preparing and Performing Shading Impact Analysis on 3D Buildings	22
4.4.5 Identify Shaded String	22
4.4.6 Generating Shading Profile.....	23
4.5 Modelling in Python:.....	24
4.5.1 Modelling Plane of Irradiance.....	24
4.5.2 Modelling Shaded_POA:.....	25
4.5.3 Modelling DC Power Output.....	26
4.6 Tools Used in the Workflow	27
4.6.1 Geographic Information Software (GIS):.....	27

4.6.2 Modelling PV System.....	28
4.7 Workflow	31
5. Results and Analysis	32
5.1 Preprocessing LIDAR Data:.....	32
5.1.1 Select Area of Interest	32
5.1.2 Classification of Point Clouds:.....	32
5.1.3 Filter Noise:	33
5.2 Generating Building Footprint:	33
5.3 Generating 3D Building Multipatch :	35
5.3.1 Roof Segmentation.....	35
5.3.2 Extrude Building in Z-Axis to Create 3D Shapes:	35
5.4 Shading Impact Analysis.....	36
5.5 Identify Areas of PV System on the Roof under Shadow	37
5.6 Estimation of Shading Profile on the String.....	38
6. Discussion	43
7. Conclusion and Future Directions	45
7.1 Research Results.....	45
7.2 Future Directions.....	45
References	47
Appendix A.....	53
Appendix B.....	58

List of Figures

Figure 1 System Loss Diagram from Aurora Solar.....	2
Figure 2 Power Losses in PV Systems	2
Figure 3 PV Plant Losses of a plant (Alhmoud, 2023)	3
Figure 4 PV Plant Losses of a plant (Alhmoud, 2023)	3
Figure 5 Illustration of Geographic Information System.....	7
Figure 6 Illustration of LIDAR Imaging.....	7
Figure 7 Illustration of Digital Terrain Map	10
Figure 8 Illustration of Digital Surface Map	10
Figure 9 Skyview Factor of a Point with Obstacles	12
Figure 10 Skyview Factor derived from Fish eye camera	12
Figure 11 Generic workflow of the study.....	15
Figure 12 LAS File in Class Symbolology.....	16
Figure 13 LAS File in Elevation Symbolology	16
Figure 14 PV Schematics of NIDA.....	18
Figure 15 PV Schematics of TETB.....	18
Figure 16 PV Schematics of QUAD	18
Figure 17 PV Schematics of UNI GYM	18
Figure 18 TYREE Energy Technology Building, UNSW	19
Figure 19 NIDA, Kensington.....	19
Figure 20 Quadrangle Building, UNSW	19
Figure 21 UNI Gym Buildings, UNSW	19
Figure 22 Noise from Point Cloud	20
Figure 23 Generating building footprint from LIDAR (Boz et al., 2015).....	21
Figure 24 LOD2 3D Buildings generated from 3D Basemaps in ArcGIS (Jayaraj and Ramiya, 2018)	22
Figure 25 LOD2 3D Buildings generated from Open Source Software (Jayaraj and Ramiya, 2018)	22
Figure 26 Sunpath Generator Tool in ArcGIS.....	22
Figure 27 Illustration of Shadow impact Analysis in ArcGIS	22
Figure 28 Shadow Impact Analysis of NIDA on Jul,5 02:31PM.....	23
Figure 29 Shadow Panels overlapped with PV Panel Polygons	23
Figure 30 PV Schematics of NIDA.....	23
Figure 31 Shadow Panels overlapped on Hillshade Analysis Layer	23
Figure 32 PV String Layout overlapped on Shadow Panel and Hillshade Analysis Layer.....	23
Figure 33 Reclassified layer output from the model.....	23
Figure 34 Detailed Workflow of the study	31
Figure 35 Area of Interest for the study.....	32
Figure 36 LIDAR clipped to Area of Interest.....	32
Figure 37 Point Clouds with Noise and Irregularities	33

Figure 38 Preprocessed LAS Dataset with point cloud reclassification	33
Figure 39 Noise Point Clouds within the area of Interest	33
Figure 40 DSM Raster.....	34
Figure 41 DTM Raster.....	34
Figure 42 nDSM Raster	34
Figure 43 LAS Point as Statistics Tool	34
Figure 44 Raster to Polygon Process	34
Figure 45 Regularized Building Footprint of TETB.....	34
Figure 46 Regularized Building Footprint of Neighbouring Buildings around TETB.....	35
Figure 47 Segmented Rooflines of TETB.....	35
Figure 48 3D Multipatch of TETB.....	36
Figure 49 Google Earth 3D Model of TETB.....	36
Figure 50 3D Multipatch of Neighbour Buildings around TETB.....	36
Figure 51 Sun positions on 21/12/2021.....	37
Figure 52 Sun positions on 25/06/2021.....	37
Figure 53 Comparison of Sun position for July and December	37
Figure 54 Shadow Impact Analysis on TETB 3D Building on the first and last hours of 21/12/2021	37
Figure 55 Shadow Panels of TETB superimposed on Hillshade Analysis	38
Figure 56 TETB Imagery georeferenced and PV Polygons on Roof	38
Figure 57 PV String 7C Shaded.....	38
Figure 58 Azimuth and Elevation for 21/12/2021.....	38
Figure 59 PV String Shade Analysis with ModelBuilder in ArcGIS.....	39
Figure 60 Shading Percentage vs Shading Factor on 21/12/2021.....	39
Figure 61 GHI vs Calculated Plane of Array on 21/12/2021.....	39
Figure 62 a) POA Shaded vs POA Unshaded. b) Shaded DC Power vs Unshaded DC Power from the string	40
Figure 63 Simulated vs Actual PV Panel DC Output from String 7C with Shading Percentage	41
Figure 64 DC Current and Voltage from String 7C to Inverter vs Modelled Shading Percentage.....	42
Figure 65 DC Voltage from String 7C vs Meteorological Data	42
Figure 66 Inverter MPPT DC Power Input vs Simulated DC Output vs Shading Percentage	43
Figure 67 Simulated Shaded DC Power vs Actual DC Power from Inverter.....	43
Figure 68 RMSE, MAE, MAPE, and nRMSE Metrics for shaded simulated vs actual DC Power Output....	43

List of Tables

Table 1 Comparison of Weather Sources.....	17
Table 2 Comparing available data from each site	20
Table 3 Comparison of GIS Software	28
Table 4 Comparision of Python IDE	29
Table 5 Tools and functions used in the study	30

List of Abbreviations

Abbreviation	Full Form
DTM	Digital Terrain Model
DSM	Digital Surface Model
DC	Direct Current
FES	Effective Shading Factor
FGS	Geometric Shading Factor
FSM	Fast Shade Model
GIS	Geographic Information System
IAM	Incident Angle Modifier
IV	Current-Voltage Curve
LID	Light-Induced Degradation
LIDAR	Light Detection and Ranging
MPPT	Maximum Power Point Tracker
NSB	Number of Shaded Blocks
NIDA	The National Institute of Dramatic Art
QUAD	Quadrangle Building, UNSW
PID	Potential Induced Degradation
POA	Plane of Array
PR	Performance Ratio
PSC	Partial Shading Condition
PV	Photovoltaic
QCPV	Quality Controlled Photovoltaics
STC	Standard Test Conditions
SVF	Skyview Factor
SAM	System Advisory Model
SAPM	Sandia PV Array Performance Model
TETB	TYREE Energy Technology Building
RMSE	Root Mean Square Error
MAE	Mean Absolute Error
MAPE	Mean Absolute Percentage Error
nRMSE	Normalized Root Mean Square Error
CSV	Comma Separated Values
Rs	Series Resistance

The underperformance of PV Systems on the DC Side
Understanding shading Effects in PV Systems using LIDAR

Rsh	Shunt Resistance
FF	Fill Factor
VOC	Open Circuit Voltage
ISC	Short Circuit Current
AOI	Angle of Incidence
PVGIS	Photovoltaic Geographical Information System
NOAA	National Oceanic and Atmospheric Administration
NASA	National Aeronautics and Space Administration
NCEP	National Centers for Environmental Prediction
NCAR	National Center for Atmospheric Research
CEC	California Energy Commission
DARTH	Data Resource Time-Series Hub

1. Introduction

In the past few decades, the global energy sector has significantly changed in favor of renewable sources. Of these, photovoltaic (PV) systems have gained a rapid growth rate worldwide. Falling costs, technological advances, and policies to lower greenhouse gases and increase energy independence drive growth. The PV market has been one of the fastest-growing global industries in recent years due to lower generation costs and local governments worldwide promoting grid-connected photovoltaic (PV) systems. (Aslam et al., 2022)

Australia has emerged as a significant force in the global solar energy market. The country's abundant solar resources and favorable policies have led to rapid PV adoption. In 2022, around 3.6 GW of new solar PV capacity was added to the grid, making up about 15% of the electricity mix in the Australian Electricity Grid. This growth is expected to continue, further establishing Australia as a leader in solar power generation (Clean Energy Report, 2023). The expansion in Australia, including residential rooftops and large-scale solar farms, is a testament to the country's commitment to sustainable energy (Shaikh et al., 2023)

With large-scale solar energy generation, monitoring these systems to ensure maximum efficiency and faultless operation is essential. While monitoring systems add to the cost, they are crucial for minimizing overall expenses in large PV installations and are even more critical for smaller plants. Performance issues in PV systems often stem from optical losses in DC components and electrical failures in both DC and AC systems. Significant problems within the DC system have been identified as leading causes of reduced output, highlighting the need for effective monitoring and diagnostics. (Alhmoud, 2023)

Understanding the performance of PV systems is crucial. Accurate performance data ensures optimal efficiency and maximizes return on investment. (Nordmann et al., 2015). Performance analysis also helps identify potential issues, such as panel degradation or system inefficiencies, which can improve system reliability and longevity. (Skomedal et al., 2021). Moreover, performance monitoring is vital for grid management, especially in regions with high solar energy penetration, enabling better forecasting and integration into the grid. (Shaikh et al., 2023)

2. Background

The increasing reliance on photovoltaic (PV) systems for renewable energy generation necessitates thorough performance analysis to ensure efficiency and reliability. As PV installations expand globally, issues such as optical losses and electrical failures have been identified as significant contributors to system underperformance.

Recent research indicates that approximately 20-25% of photovoltaic (PV) systems experience underperformance, often due to soiling, shading, and component degradation. These factors can lead to up to 30% energy losses in affected systems, particularly in regions with high dust levels or suboptimal maintenance practices. (Aslam et al., 2022). Furthermore, a study revealed that nearly 10% of installed PV

systems suffer from electrical faults that can reduce efficiency by 15–20% if not promptly addressed. (Pillai et al., 2019) . These statistics highlight the necessity for rigorous performance analysis to mitigate losses and optimize PV system efficiency.

3. Literature Review

This section discusses the approach of identifying the causes and the share in the reduction of PV output due to various underlying factors. The following sections will provide a preliminary study of shadowing effects on PV systems, with a brief analysis of temporary and permanent obstructions on the PV system. As part of this chapter, different methodologies and models are used to estimate shading impacts. We also propose a research gap, including both traditional empirical approaches and more advanced mechanisms such as LIDAR-based analysis or simulation models. This gap is not just a point of interest but a crucial aspect that requires the attention and contribution of all involved in the field of PV system performance analysis.

3.1 Overview of the causes of loss of performance in Photovoltaic Power Plant

PV solar power plants encounter suboptimal performance due to various optical and electrical losses Figure 1. The optical losses are caused by reduced irradiance on the PV panel, partial shading losses, far shading losses, near shading losses, incident angle modifier (IAM) losses, soiling losses, potential induced degradation (PID) losses, temperature losses, light-induced degradation (LID) losses, PV yearly degradation losses, and array mismatch losses which predominantly occurs on the DC components of the PV system. The impact of shading on the performance of PV solar systems. It notes that even partial shading of a solar panel can significantly reduce its output and that shadowing on one panel can affect the production of the entire string or module. The research presents a case study in which shadowing reduced the energy yield of a PV solar system by up to 50%. (Alhmoud, 2023)

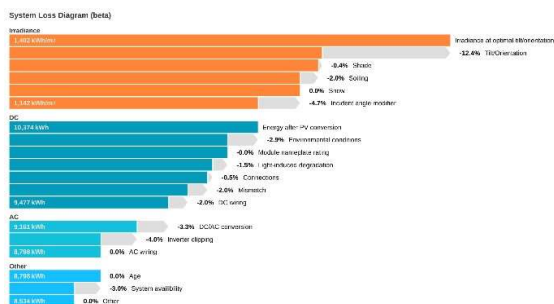


Figure 1 System Loss Diagram from Aurora Solar

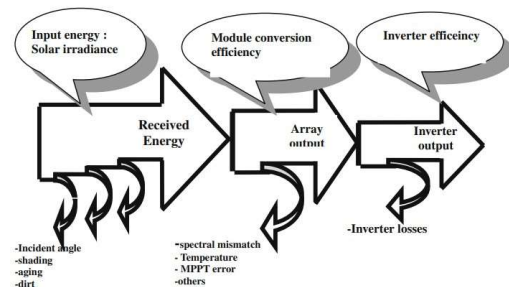


Figure 2 Power Losses in PV Systems

The electrical losses have been classified into DC plant and AC plant losses. (Alhmoud, 2023)

DC Plant Losses: This includes losses such as environmental conditions (Temperature, Wind Speed), Light-Induced Degradation of the PV Module, Cable Losses, Diode Losses, mismatch losses caused by temperature, and faults occurring on the DC components on the PV system.

AC Plant Losses include losses such as the inverter, transformer, and transmission line losses. These losses can impact the efficiency and performance of the solar cells and the overall system.

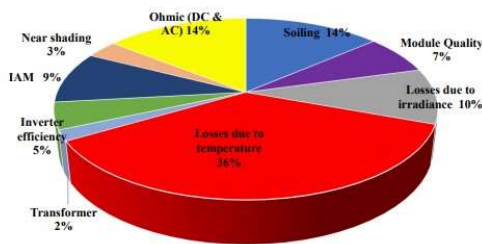


Figure 3 PV Plant Losses of a plant (Alhmoud, 2023)

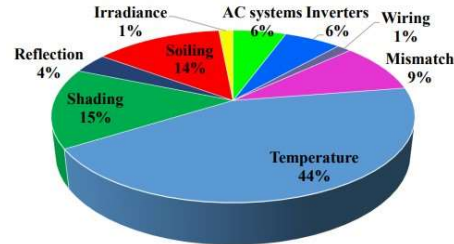


Figure 4 PV Plant Losses of a plant (Alhmoud, 2023)

3.2 Causes of DC Losses in PV Plants

Degradation of PV Module

Over time, several external factors can cause a gradual decline in the performance and efficiency of photovoltaic (PV) systems. These factors include temperature, humidity, UV exposure, and mechanical stress. Furthermore, potential-induced degradation (PID) can occur due to voltage stress on PV modules, leading to performance degradation. Another factor is light-induced degradation (LID), which can occur in certain types of PV cells, causing a decrease in performance under initial exposure to sunlight. (Munoz et al., 2011).

In addition to PID and LID, other potential factors such as corrosion, delamination, and encapsulant discoloration can also contribute to PV degradation. These factors can reduce the system's overall output, negatively impacting its efficiency and lifespan. Therefore, monitoring and maintaining the PV system regularly ensures optimal performance and longevity. (Jordan et al., 2017).

Module Temperature

Module temperature significantly influences PV module performance. As the temperature rises, the conversion efficiency of PV modules generally decreases, leading to a decline in actual performance. (Dash and Gupta, 2015). The temperature positively impacts short-circuit current but has a negative impact on open-circuit Voltage and Power output.

Various studies have shown that as the solar cell temperature increases, its output power decreases by about 0.37 W, and its electrical efficiency reduces by 0.06% for every one °C rise. In addition, it has been observed that the temperature of the solar cell increases by 4.93°C and 2.64°C, respectively, for every 100 W/m² increase in irradiation with and without a cooling system. Finally, at an irradiation of 1000 W/m², the electrical efficiency of solar cells decreases by 0.06% for every one °C increase in temperature. (Rahman et al., 2015). These findings highlight the importance of maintaining optimal operating temperatures for solar cells to achieve maximum efficiency and output power.

Fill-Factor

Minimizing the fill factor loss is crucial to maximizing the efficiency of solar PV modules. Fill factor loss refers to the decrease in the fill factor of a solar cell, which can be caused by various factors such as series resistance (R_s), shunt resistance (R_{sh}), and J02 recombination. (Khanna et al., 2013). The fill factor (FF) is a critical parameter of a module that determines the effectiveness, and it should be as close to unity as possible on the I-V curve. The fill Factor is the ratio of the maximum power (P_{max}) of a solar PV module to the product of its open circuit voltage (VOC) and short circuit current (ISC). By optimizing the fill factor, we can enhance the performance of solar PV modules and make them more efficient. (Sharma and Purohit, 2014).

Soiling

Soiling refers to accumulating dirt and pollutants on photovoltaic modules, which can reduce their efficiency and energy production. (Pavan et al., 2011). It forms a thin screen over a module and thus minimizes the light capture of the PV panels. Different types of dust, including sand, ash, red soil, limestone, calcium carbonate, and silica, have varying impacts on PV performance. (Al Siyabi et al., 2021). A study found that the losses contributed by soiling in dry areas would reach up to 15%, leading to a significant drop in Annual Yield if not maintained. (Zorrilla-Casanova et al., 2013).

Potential Induced Degradation

High voltages between the PV cells and the module's grounded frame primarily cause PID. This voltage stress can result in the migration of charged particles within the module, leading to performance degradation. (Jordan et al., 2017). PID-shunting (PID-s) is the most common type of PID in conventional p-type c-Si PV modules. It is closely associated with reduced shunt resistance (R_{sh}) and increased dark saturation current due to recombination in the space-charge region. Sodium ions (Na) play a prominent role in the evolution of PID-s, causing shunting and efficiency degradation. (Luo et al., 2017). Potential induced degradation (PID) is a performance degradation mechanism in PV systems due to stray currents, leading to a gradual loss of power of up to 30% or more. PID generally occurs in PV systems with ungrounded inverters (Kim et al., 2021)

PV Module Orientation and Tilt Angle

PV module orientation has different impacts on grid operation, including power gradients, voltage issues, and asset overloading. Overall, the choice of PV module orientation should consider the trade-off between peak power reduction and energy yield to minimize losses. (Tröster and Schmidt, 2012). Optimizing PV module performance under inhomogeneous soiling conditions, including mounting orientation, can lead to up to 65% higher output power. (Hanifi et al., 2020).

Shading

Shading losses refer to reduced solar energy output caused by obstructions such as buildings, trees, or other objects that cast shadows on solar panels. By reducing the amount of sunlight that reaches the panels, shading can significantly impact the performance of a solar photovoltaic system. (Pachauri et al., 2021) Shading can significantly damage traditional crystalline PV modules, leading to performance differences among PV cells and potentially permanent damage to the modules. (Zsiboracs et al., 2021), causing a reduction in the annual energy yield from the Solar PV Plant. A study (Breckl and Topič, 2011) It was found that 100,000 roof programs showed a decrease in the annual energy yield due to shading.

3.3 Preliminary Study

3.3.1 Shadowing Effects on PV

When a PV module is partially shaded, the shaded cells can act as resistors, reducing the module's overall voltage and power output. Shading effects can also cause hotspots in the PV module, damaging and reducing module life. Careful site selection, module placement, and design considerations are essential to minimize shadowing.

Partial shading conditions (PSC) in a photovoltaic (PV) array can result in power losses due to a mismatch in PV module characteristics. Shaded modules receive lower irradiance levels and have reduced current output compared to unshaded modules. (Saiprakash et al., 2021)

3.3.2 Current Estimation Techniques for Shading Losses in PV

Several research works were implemented to estimate the shading occurring in the system through sensory and non-sensory approaches. Shading models that estimate the drop in annual yield and performance due to full shading and partial shading conditions have been implemented to understand better the reversible and irreversible performance drops occurring in the system.

The study by (Satpathy and Sharma, 2020) discusses a novel technique to detect partial shading in solar PV systems without disconnecting the load. The method uses the voltage difference across each row of the PV array to indicate shading severity. The study also proposes a static and dynamic reconfiguration

method to mitigate the effects of shading and enhance the power output. However, this avoids the conventional methods of detecting partial shading on short circuit current (I_{sc}) by isolating the load from the PV array. This is impractical and undesirable for large-scale or stand-alone PV systems. Implementing this technique on MATLAB using a 3x4 120W polycrystalline PV array showed successful detection of PSC on time.

On analyzing the study of (García et al., 2003) The paper proposes a mathematical shading model to estimate the reduction of annual yield due to shading in photovoltaic (PV) systems. The model is based on the calculation of the influential shading factor (FES), which depends on the shaded fraction of the array area (FGS) and the number of blocks affected by shade (NSB) (A block is a group of solar cells protected by a bypass diode) The model is applied to the directional components of the in-plane irradiance, such as direct and circumsolar radiation. Experimental measurements on multiple photovoltaic arrays with different configurations and shading profiles validate the model. The method has been validated by a broad experimental testing campaign on several shaded PV arrays with different configurations and shading profiles. The results show that the method performs better than other existing models.

Correspondingly, the IV Curve of the module is used in (Skomedal et al., 2020) to estimate the performance of a photovoltaic (PV) module under partial shading conditions based on an explicit analytical model. This method uses only I-V data from the manufacturer or measured at reference conditions. It derives a direct voltage expression in terms of current for a single PV cell, a submodule, and a PV module. Experiments in different outdoor shading scenarios verified the effectiveness of this method. The method is fast and accurate and can predict power generation, evaluate MPPT strategies, and design control schemes for PV systems.

Based on the reviewed studies, shading on PV panels can be detected by analyzing the system's IV profile and power parameters after the installation process. (Zhang et al., 2021). However, a more practical approach for estimating shading conditions would be to consider the shading needs of the PV system at a given location and orientation, which would help improve the accuracy of annual yield estimations.

The method proposed by (Goss et al., 2014) uses the shading loss algorithm to generate an irradiance map of the array for each time step for individual cells or cell portions. The horizon datum and the PV array layout are translated into a dome of sky patches, each with a Boolean value indicating the state of shaded or unshaded by any obstruction. The model then uses a time series simulation, where the irradiance map for each cell or cell portion is calculated for each time step based on the sun position and the sky-patch status. The model's validation against two chimney shading scenarios showed an error of less than 1%. The model is also optimized for different sky-patch resolutions and computation times. The model can be integrated with cell performance and energy yield models to account for the shading losses due to partial or complete shading of PV arrays.

The method proposed by (Capdevila et al., 2013) Uses a shading analysis tool embedded in a CAD software environment. The tool can model the shading effects of arbitrary tracker geometries, module layouts, and string concatenation schemes. It can also account for the topographical features of the site based on digital elevation model data. The tool calculates the shadow fraction of each area element of the tracker at any time step. Then, it solves the equivalent circuit to estimate the electrical shadow loss—the tool claims to improve the accuracy of energy conversion predictions for one and two-axis vertical trackers.

An advanced technique that uses a video camera to track shading across the day has been implemented by (Meyers et al., 2016) ; the study presents a parameterized shade loss model called the "Fast Shade Model" (FSM) that allows for the calculation of system-level power loss based on three input parameters. Shading is estimated by creating a model of the test system in SketchUp using geolocation and shadow-casting features. Images of the shade on the array at any time of interest are built using Ruby scripting in Sketchup and subsequently analyzed using Python script to determine the area of each shaded cell. This approach demands time-stamped imagery and building models to study the sun's path and estimate shading on PV systems.

3.4 LIDAR and GIS Technology

Geographic Information Systems (GIS) are technologies that merge spatial or geographic data like maps, satellite imagery, and LiDAR data with attribute data such as land use, population, and infrastructure. They enable the analysis, visualization, and comprehension of patterns and relationships in the real world. GIS allows capturing, storing, manipulating, analyzing, and presenting geographically referenced data. (Nguyen et al., 2012a)

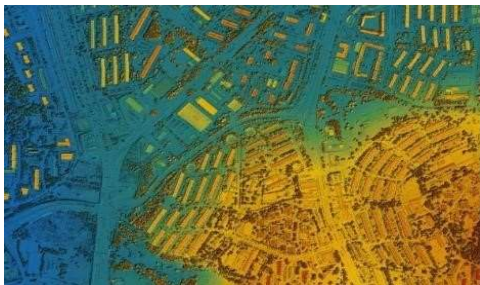


Figure 5 Illustration of Geographic Information System

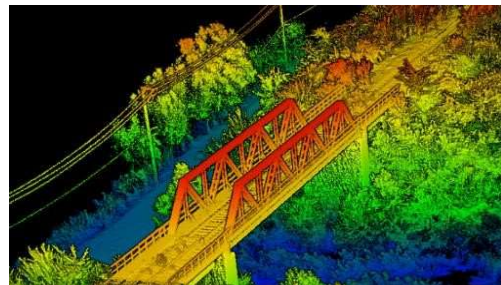


Figure 6 Illustration of LIDAR Imaging

LIDAR, or Light Detection and Ranging, is a remote sensing technology that uses pulsed laser light to measure variable distances to the Earth's surface (Lukač et al., 2014). Currently, LIDAR has various applications in remote sensing, including autonomous vehicles, weather forecasting, astronomy, and more. This technology uses a laser beam emitted from a sensor and directed toward the target. The laser beam reflects off the target and returns to the sensor, where it is detected and measured. Lidar accurately determines the distance to a target by measuring the time a laser beam travels to and back to the target.

It has a potential application in renewable energy planning by analyzing the shadowing effects and identifying suitable locations for solar installations by combining 3D models of the urban environment with sun position data, which allows for the calculation and visualization of shadows cast by buildings.

3.5 Application of LIDAR and GIS in the Renewable Energy Industry

Site Selection and Resource Assessment:

GIS and LIDAR technology can determine suitable locations and estimate the potential of renewable energy resources for renewable energy projects such as wind farms, solar farms, or hydropower plants (Abd Latif et al., 2012). Through analysis of various factors in meteorological data sources such as wind speed, solar radiation, topography, land use, and environmental constraints, GIS and LIDAR can help optimize the site selection process and provide accurate and detailed information on the availability and variability of the resources, which is essential to reducing risks and ultimately minimizing costs associated with these projects. (Radosevic et al., 2022)

Environmental impact assessment:

On analyzing processed data sources like biodiversity data, land use data, and social data, the environmental impacts of renewable energy projects on wildlife, ecosystems, and cultural heritage are studied. Implementing this model during the pre-assessment of a project helps identify the vulnerable areas and could suggest mitigation measures to reduce the negative impacts. During the operation and maintenance phases, the processed information of GIS and LIDAR helps monitor the environmental performance of renewable projects. (Xie et al., 2022)

Asset Management

Renewable energy assets, like wind turbines, solar panels, or hydroelectric generators, can be effectively monitored and managed using GIS and LIDAR technologies. By analyzing real-time data, such as SCADA data, weather patterns, or maintenance information, GIS and LIDAR can assist in optimizing the performance and upkeep of these assets, ultimately enhancing their reliability and efficiency. (Schultz, 2012)

The technology is also utilized to monitor the structural soundness of assets and identify any defects or damages that may impact their performance or safety. Using different types of sensors like accelerometers, strain gauges, or thermal cameras, GIS and LIDAR can supply precise and timely information regarding the condition of assets, which can help prevent failures or accidents. (Zhong and Haiyan, 2023). The processed information from the sensors, combined with predictive analytics via Machine Learning and AI, would help schedule and optimize maintenance strategies that ensure the structural integrity of the project's components.

3.6 Estimation of Shading and Annual Yield through LIDAR

Studies and research have utilized LIDAR and GIS technology to address challenges in the solar and wind energy industry. The previous sections focused on addressing the reasons behind the subpar performance of PV on the DC side. As a potential solution, LIDAR and GIS have been examined to understand better the current models for shading and estimating energy yield. Various researchers have developed solar radiation models that utilize LiDAR data and GIS tools to calculate the direct, diffuse, and reflected irradiances on urban surfaces while considering the shading effects of the surrounding environment.

A study by (Gawley and McKenzie, 2022) They investigated the effectiveness of using GIS and orthophotography datasets as components of GIS to model the energy yield of PV systems on rooftops. The study adopted a methodology that involved comparing and analyzing the digital surface models (DSM) derived from light detection and range (LiDAR) and orthophotography DSM data using UK-standardized PV formulas. The methodologies from various studies have been analyzed to understand the PV annual yield estimation through shading models generated from Skyview Factor derived from Raster DSM and DTM data generated from LIDAR and GIS datasets.

3.6.1 Digital Terrain Map (DTM)

Digital Terrain Model (DTM) models the earth's surface without structures like buildings, vegetation, or other objects. It only includes natural terrain features such as hills, valleys, and plains, essential in understanding natural terrain features, modelling water flow, assessing landslide risks, and planning environmental studies, civil engineering, and land use planning. DTM contains crucial and accurate terrain information without any impact on natural or artificial objects. (Nguyen et al., 2012b)

3.6.2 Digital Surface Map (DSM)

The DSM (Digital Surface Model) plays an essential role in the learning process for estimating solar PV (photovoltaic) capacity in urban areas. It can be used to represent urban landscapes and buildings accurately and accurately, and it has resulted in an accurate model of sunlight with shading effects. DSM typically uses raster sizes in the range of 0.3 m to 1 m and is ideal for assessing existing solar rooftops in urban areas (Freitas and Brito, 2017). By simulating shading effects, especially during the summer months, the study could identify potential losses in solar irradiance due to shading from surrounding buildings and other features captured in the DSM. (Yousuf and Siddiqui, 2018).

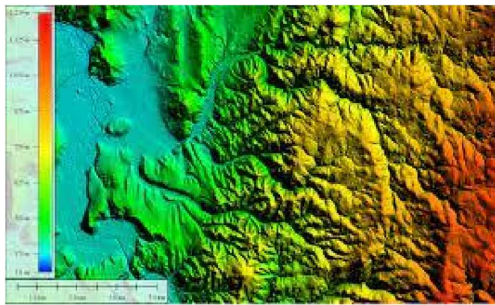


Figure 7 Illustration of Digital Terrain Map

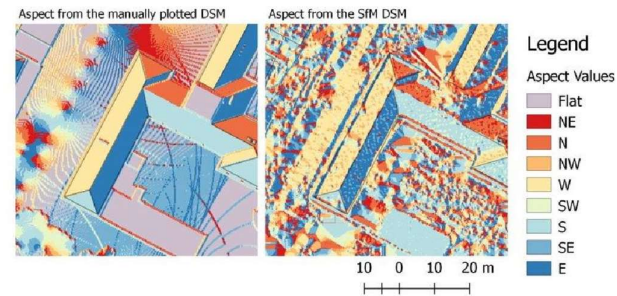


Figure 8 Illustration of Digital Surface Map

3.7 DTM and DSM-Based Shading Models

Pixel-Based Shading Model: Pixel-based shading models in computer graphics are often used to define the color of each pixel in the generated image. They calculate the color of each pixel using lighting conditions, object surface type, and camera position. In PV shading, pixel-based shading models can be used to estimate the shading effect of nearby objects on the solar irradiance of a PV module. (Li et al., 2016). The model divides the sky dome into smaller components and calculates luminosity, and each element gets calculated. In addition, it considers the effect of nearby obstacles on the beam and the propagating radiation component. According to a study (Yousuf and Siddiqui, 2018) The proposed method is straightforward, accurate, and applicable to existing and future buildings.

Vector-Based Shading Model: The vector-based shading model estimates the outcomes of shading surrounding objects at the sun irradiance of photovoltaic (PV) modules. The model considers buildings, trees, and terrain capability-shading objects and applies a voxel filter to reduce the factors inside the LiDAR information. (Liao et al., 2019). The paper proposes a clear-sky coloration index to compare the shading results on extraordinary surfaces. The model uses a voxel clear-out to reduce the factors inside the LiDAR statistics and Delaunay triangulation to create a mesh of shading triangles. The paper (Lingfors et al., 2018) It also discretizes the roof sides into grid points and estimates shading by projecting them along vectors pointing at sky sectors.

SOL Algorithm: The SOL model is a LiDAR-based method that calculates hourly solar radiation for each site in a digital surface model (DSM) and estimates shadows caused by surrounding buildings and vegetation. The algorithm uses airborne LiDAR data DSM to model solar radiation on the roof. SOL models are more accurate and efficient than others and can handle complex urban features more accurately (Freitas and Brito, 2017).

The paper also compares the results of SOL with other shading models. In PV shading, the SOL model can estimate shade loss in PV arrays and optimize the installation of PV modules on rooftops. The SOL model (Li et al., 2015) Compares the results with other shading models to calculate the solar radiation of rooftops in San Francisco.

Ray-tracing algorithm: Ray tracing is used in computer graphics to create realistic lighting effects in a virtual environment (Tian, n.d.). The model calculates the color of each pixel based on the light path falling on objects in the digital surroundings; the pixel contains the skylight values for each sky band, determining the incident radiation at the sensor points. The algorithm is a heavily hardware-intensive task and is critical based on the computed resolution and density of the pixels. (Liao et al., 2019)

Hillshade Analysis FROM Arc GIS: Hillshade analysis is a beneficial feature in ArcGIS that generates a shaded comfort raster from a floor raster by considering factors that include the angle of the illumination source and shadows. Hillshade evaluation estimates the shading outcomes on PV modules. (Gawley and McKenzie, 2022). The paper also proposes a new technique for deciding on the most desirable rooftops for PV setup based totally on the consequences of hillshade analysis. (Li et al., 2015). Additionally, it utilizes hillshade evaluation to estimate the solar capability of rooftops in urban regions. This author also uses a viewshed analysis to perceive the visible and shaded areas of the rooftops and a solar radiation version to estimate the sun irradiance on the rooftops.

Multiresolution shadowing: The multi-resolution shading model calculates the shading effect of the surrounding environment on solar radiation in photovoltaic (PV) modules. The model considers low-resolution and high-resolution grids of land and buildings, used to calculate the shadow parameters of each cell in a grid generated from LiDAR data -it is more efficient and accurate than using a grid; it can capture the shadow effects of environmental and urban factors area. (Lukač and Žalik, 2013), also accounts for explicit shade vegetation using the leaf area index. Grid generated using LiDAR data using a spatiotemporal multiresolution-based shading method to calculate shading coefficients for each cell. (Lukač et al., 2014). This paper also compares the results of the proposed method with other shading models to confirm its accuracy.

QCPV-Tuning model: The QCPV-Tuning model is a method used to calculate the effect of shading in photovoltaic (PV) systems. The model derives module orientations and losses from quality-controlled PV power generation data and uses a tuning routine to correct cyclic systematic deviations due to shading. (Killinger et al., 2017). The QCPV-Tuning model can help calculate shading losses in PV arrays and could provide PV installation of sound modules on roofs. In a study (Lingfors et al., 2018)The QCPV-Tuning model is compared with other shading models to calculate shading losses in PV arrays. Based on the QCPV-Tuning model results, the paper also proposes a new method to select the optimal roof for PV installation.

Skyview Factor:

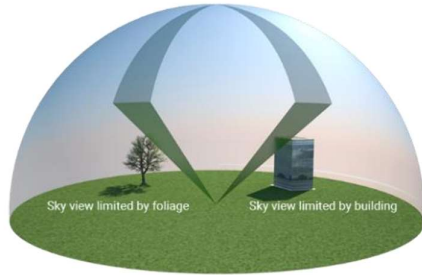


Figure 9 Skyview Factor of a Point with Obstacles



Figure 10 Skyview Factor derived from Fish eye camera

Skyview Factor: SVF measures a location's openness to the sky, which directly influences the amount of solar radiation a surface receives. In solar Energy studies, SVF is used to estimate the shading effect on building surfaces (facades), which is included for accurate solar irradiance calculation. (Nguyen et al., 2012a). SVF model potentially replaces the relatively slow and hardware-intensive vector-based shading analysis. Also, it models the shading factor on the roofs and facades to estimate the annual solar insolation on the facades of the building effectively. DSM Rasters have been modelled to calculate SVF for a given time and day of the year. Sun Path tool integrated with DSM Rasters estimates the SVF of a given point across the year. (Yousuf and Siddiqui, 2018).

Based on the observations of the above studies, the analysis model's performance varies based on the location and the data sensitivity.

3.8 Research Gap

Although considerable progress has been made in both photovoltaic (PV) technology and shading analysis, there are still some critical areas that most existing methodologies fail to handle well enough. This eventually prevents a complete solution from being provided to reduce the underperformance of PV strings due to shading.

To improve the long-term reliability of the system, the underlying impacts of shading effects, such as power losses due to Hotspot Effects, on PV panels and the resultant system efficiency caused by shading, especially in urban environments, could be studied. Such gaps are evident when looking at the use of LiDAR technology in shading analysis across the DC side of PV systems. The study gaps identified are:

3.8.1 Limited Utilization of LiDAR with Performance Models:

The solar PV Industry has been accommodating Lidar technology for estimating annual energy yield by using Point Cloud Data from LiDAR Mapping Sources and identifying potential obstructions that could impact solar irradiance. However, its application to understanding the impacts of shading analysis from a string level remains unexplored.

One of the studies that included the LiDAR scanning technology applied by (Bocullo et al., 2023) It was a successful tool for evaluating the potential shading impacts on a location's solar PV array. Moreover, it was a significant element used in conjunction with UAV photogrammetry to understand how the shading impact on all units of Lithuania might be reduced. The study showed the layout optimization to avoid shading, which, in turn, focused on the aspects of system yield rather than the performance of individual strings in the array.

Another study (Lingfors et al., 2018) Models a set of PV Systems through LiDAR and performs shading analysis to estimate the overall simulated yield in comparison to the actual yield. However, observing the PV System output fails to address the impact of shading caused on a string level from the DC Side, which would be necessary to address the long-term performance impact on the system.

3.8.2 Underdeveloped Predictive Analytics for Shading Impact:

Current shading studies using LIDAR mainly focus on static shade impacts but fail to estimate the dynamic nature of shading patterns due to seasonal changes, weather variability, and the movement of surrounding objects.

Although some previous work with shading estimations (Lingfors et al., 2017) It identifies the shading regions through roof segmentation and modelling from LiDAR but does not account for the impact of PV systems on dynamic shading objects throughout the year.

(Vega-Garita et al., 2023) Discusses a novel approach to assessing the impact of shading in PV Systems by extracting the skyline from the smartphone. However, this method uses a static snapshot from a panoramic image captured by a smartphone along with LIDAR. This mythology does not consider the impact of the sun's movement across various seasons in a year.

The suboptimal performances of the PV array/string failed to be recognized due to a lack of real-time monitoring systems that use LIDAR to dynamically adjust PV operational parameters to identify and mitigate the causes of underperformance.

3.9 Summary

The above section conducted an up-to-date literature review of the existing studies. Firstly, the literature review identifies the types of losses in a PV System. After further studying the underlying factors, the study also focuses on the causes and effects of PV Performance losses due to various environmental and system-level factors.

Further downsizing our research domain to shading losses, which account for up to 10 to 30% of the losses, the literature review includes studies on understanding the PV System performance of variable types of shading, leading the study to focus on the existing estimation techniques employed for shading on PV Systems.

Studies on various conventional techniques of estimating shading extent on PV Panels, such as using Solar Assessment Tools like Solar Pathfinder, Solmetric Suneye, and other software tools such as PV syst and SAM, were understandable to be deployed on small geographical extents. The studies on the estimation of shading techniques did not involve comparing the performance of a PV System on the DC side, leading to further diversification of the study towards LiDAR-based estimation of PV System Performance.

A Literature review was performed on Various studies that employed the LiDAR technologies focussed on annual yield-based performance analysis through various LiDAR processing techniques and diverged to the current methodologies on shadow estimation methods. However, the importance of a PV system performance from the string level to further increase the system operating efficiencies through pre-estimation of shading points on PV Panels across the year would result in reducing the impact of shading-related power losses due to hotspots, therefore increasing the Long term reliability of the PV Systems through improvised monitoring strategies to detect temporary and permanent constraints on the PV Panel.

In the upcoming sections, LiDAR data will be utilized to develop time-series shadow estimation techniques to analyze the impact of shadows on the power generation of a PV string throughout the day.

4. Experimental Methods

Introduction

Shading caused by surrounding structures like building facades, when accurately identified and their impacts being quantified on a PV String through LIDAR Data, would reduce the DC power output from the PV System. This reduction in performance is directly proportional to the extent and duration of shading, leading to measurable losses in energy yield at a given period. By effectively mapping and analyzing the shading patterns, predicting and mitigating these losses through layout updates will likely optimize the overall efficiency of PV installations and gain a deeper understanding of the reaction to Power output due to the shading effects.

The table below shows the breakdown of the hypothesis and the motive of our study.

Cause	Shading caused by surrounding Structures
Measurement Tool / Sources	LIDAR Data is used to identify and quantify the dimension and spatial orientation of surrounding structures
Effect	Reduction in the DC Power output from the string

Proportional Relationship	The reduction in the DC Power output's performance is hypothesized to be due to the extent and duration of shading.
Objective	The goal is to estimate and understand the shading impact on the DC side of the PV system, mitigate these losses, and improve PV Systems' efficiency.

This section will outline a brief methodology for addressing the issue of rooftop shading from a broader perspective. A good data source is essential for estimating the shading regions of rooftops effectively and reliably.

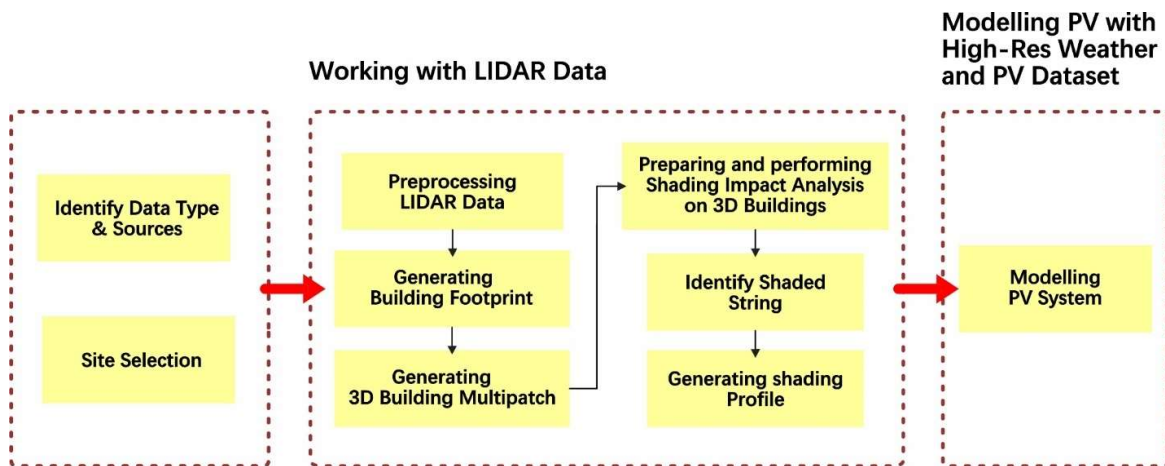


Figure 11 Generic workflow of the study

The flowchart shown in Figure 11 is crucial in providing a visual sequential order of sections that progress the study flow, starting with identifying required data types and ending with validating and calibrating the results. It serves as a guide, ensuring a systematic and comprehensive approach to the study.

4.2 Identifying Required Data Types and Potential Sources

LiDAR: High-resolution Lidar data is essential for accurately modelling a three-dimensional map of the area to be studied. The resulting point cloud from LIDAR data would contain a million data points that capture objects' spatial information and dimensions, such as building blocks, trees, and other shading potentials. The high level of LiDAR is crucial for pre-classifying point clouds into various classes, such as Buildings, High Vegetation, Medium Vegetation, and Low Vegetation, for estimating shading impacts on photovoltaic (PV) systems because it provides a detailed and precise representation of the surrounding environment. (Gergelova et al., 2020)

ELVIS is a platform offered as a collaboration between DCS Spatial Services and GeoScience Australia to deliver high-quality and valuable Elevation and Point cloud data used widely across various sectors, such as engineering, energy, and environmental management.

Figures 12 and 13 below show the LAS LiDAR Point cloud of UNSW, Kensington Campus, segregated by elevation color code. The raw LAS data is sourced from the GeoScience Australia platform and accessed through the Elevation and Depth portal, which provides free access to high-quality elevation data, LIDAR Point Clouds, and the Digital Elevation Model (DEM).



Figure 12 LAS File in Class Symbology

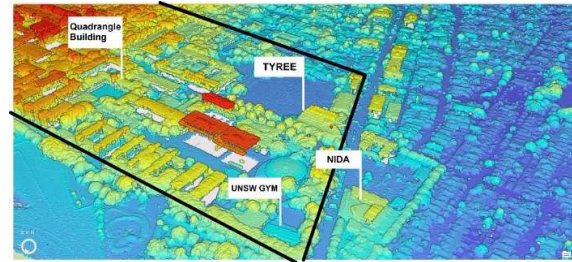


Figure 13 LAS File in Elevation Symbology

Meteorological Data:

Post-modelling the 3D objects from LiDAR, the high-accuracy meteorological Data containing key parameters are required to simulate a PV Plant's ideal and shaded conditions. Parameters such as Solar Irradiance in the form of GHI, DHI, and DNI are needed to determine the PV Plant output; other parameters such as Air Temperature, Windspeed 10m, and Cloud cover are required to compute Module Cell Temperature that adversely impacts the PV Power output. Additionally, the meteorological data would be evident in validating and calibrating LiDAR-based models, ensuring the reliability and accuracy of the study. The table below compares different sources and the origin and variability of weather data parameters.

	Source	Data Acquisition	Variability	Accuracy	Accessibility
1	BOM (Bureau of Meteorology)	Primarily ground-based weather stations, satellite observations, and radar systems within Australia.	High spatial and temporal variability due to the dense network of ground stations and advanced forecasting models.	High accuracy within Australia due to localized data collection and advanced meteorological modelling. (Govekar et al., 2022)	It is freely accessible to the public, but some specialized data products may require a subscription or request.

2	SOLCAST	Satellite data (e.g., Himawari-8), ground-based stations, and proprietary algorithms for solar radiation and weather forecasting.	Moderate variability; provides high-resolution data (1-5 km grid) with updates every 5-15 minutes.	High accuracy for solar radiation forecasts, particularly in regions with strong satellite coverage. Accuracy may vary in areas with less frequent satellite updates. (Pham et al., 2022)	Data is accessible via API with free and paid tiers; full access requires a subscription.
3	PVGIS (Photovoltaic Geographical Information System)	Uses satellite data (e.g., Meteosat), reanalysis data, and ground-based stations for solar radiation and climatological parameters.	Low to moderate variability; provides data at a lower resolution (3-4 km grid) with historical datasets available.	Generally accurate for long-term solar energy predictions, though short-term forecasts may have lower precision. (Sayago et al., 2020)	Freely accessible to the public through a user-friendly web interface and API.
4	NASA	Satellite data (e.g., MODIS, CERES), reanalysis datasets (e.g., MERRA-2), and ground-based observations.	Moderate variability with global coverage offers high-resolution (1-10 km grid) and lower-resolution data depending on the dataset.	High accuracy for global scale meteorological data, though localized accuracy may vary based on the resolution of the dataset used. (Liu and Matolak, 2018)	It is accessible to the public through various portals, including NASA POWER and Earthdata, with APIs available.
5	NOAA (National Oceanic and Atmospheric Administration)	Satellite data (e.g., GOES, JPSS), ground-based stations, buoys, and reanalysis datasets (e.g., NCEP/NCAR).	High variability due to extensive global network and frequent updates.	High accuracy for global and regional forecasts, with comprehensive models and data assimilation techniques improving reliability.	Freely accessible to the public through multiple portals and APIs; specialized data may require a subscription or data request.

Table 1 Comparison of Weather Sources

On comparing the sources and various studies such as, ("Solcast," 2019) and (Yang and Bright, 2020) Validate Solcast's improved Data quality and consistency and its utilization for research across various sectors compared to other sources. Considering the 5-minute periodical availability of historical data, validating the PV performance from the string would be essential. Critical parameters such as GHI, DHI, DNI, Air Temperature, wind speed_10 m, Cloud Coverage, and Zenith Angle were requested from 01-01-2020 to 04-07-2024.

PV System Data and Schematics:

PV system data is crucial for accurately estimating the impact of shading on photovoltaic (PV) systems when using LIDAR technology. This data encompasses various parameters that directly influence the performance and efficiency of PV installations.

PV System Schematics: A detailed diagram that visually represents the layout and components of the installed PV System. The schematics document is essential to understanding the nameplate details, such as the system's rated capacity, including the tilt and orientation of the PV System. The document would have a detailed illustration of a single-line diagram explaining the connection layout of the active and passive components on both the DC and AC sides.

The PV Schematics of the TETB Building and UNI-GYM were obtained from DARTH administrators, and the PV schematics of NIDA were procured from the NIDA Sustainable Manager and are shown in Figure 14-17.

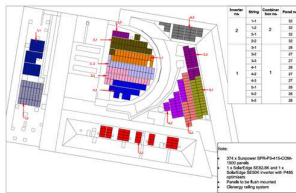


Figure 14 PV Schematics of NIDA

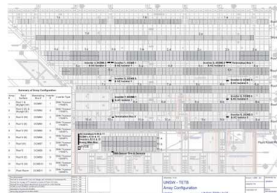


Figure 15 PV Schematics of TETB

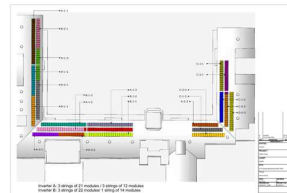


Figure 16 PV Schematics of QUAD

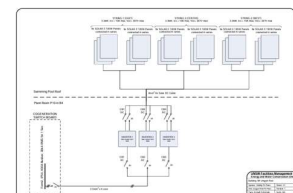


Figure 17 PV Schematics of UNI GYM

PV System Data: Primary data were chosen based on site selection. However, since the study aims to analyze the string-level DC Power Performance from an actual system, central potential site locations only had the Inverter AC output.

DARTH (Data Resource Time- Series Hub) is an Energy Database that includes critical site data like PV Generation, building energy consumption, and weather data gathered across buildings in the UNSW Sydney campus and other home properties across Australia. The DARTH is easily searchable and continually updated with real-time data, vital for enhancing research activities in renewable energy and future electricity grids.

PV System data for site locations like TETB and UNSW GYM were accessed from DARTH, which has data on 5-minute intervals, which is essential for high-sensitivity PV Power analysis. However, the DC Parameters of the inverters have been accumulated only in the TETB building.

4.3 Site Selection

A carefully chosen site is required to ensure that the study captures a wide range of relevant shading scenarios due to temporal and permanent obstacles, which would produce accurate and reliable data. By considering Factors such as shading diversity, solar exposure accessibility, and environmental impact, the study could maximize the effectiveness and applicability of the outcomes. [state a study]

The underperformance of PV Systems on the DC Side

Understanding shading Effects in PV Systems using LIDAR

Complex urban rooftops were initially considered for study to better understand the effects of shadowing on PV panels. Some potential sites included the PV Systems on the rooftops of TETB, NIDA, QUAD, and PV GYM, as shown in Figures 18-21. However, before the start of the study, an analysis based on the availability of required data for each building was weighed, and a rooftop was chosen.

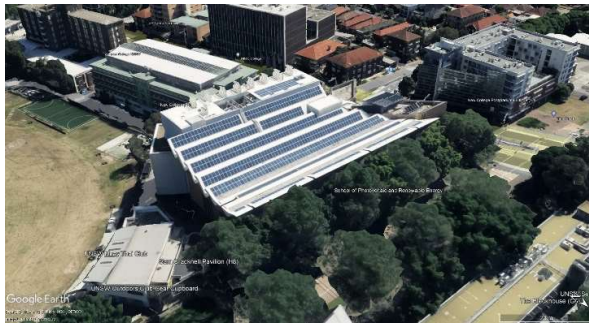


Figure 18 TYREE Energy Technology Building, UNSW



Figure 19 NIDA, Kensington



Figure 20 Quadrangle Building, UNSW



Figure 21 UNI Gym Buildings, UNSW

The table below shows the weighing of choice based on data availability. The choices are weighed based on the availability of

1. PV Schematics
2. LIDAR Data
3. Meteorological Data
4. PV System Data (DC Parameters)

S.No	Building	PV System Rating	LIDAR Data	Meteorological Data	PV System Data	Score
1.	NIDA Buildings	155.21kWp	1	1	0.5 (contains only AC Parameters)	2.5

2.	TETB	141.92kWp	1	1	1 (contains both AC and DC Parameters)	3
3.	Quadrangle Building	100kWp	1	1	0	2
4.	UNSW Fitness Center	9.9kWp	1	1	0.5 (contains only AC Parameters)	2.5

Table 2 Comparing available data from each site

Based on the score for data availability, the TYREE Energy Technology Building (-33.9175, 151.2268) has been chosen, as it outpaces other buildings due to the system's availability of DC Parameters. The schematics of the 141.92kWp PV plant of TETB are attached in Appendix A.

4.4 Working with LIDAR

The workflow presented in Fig outlines a proposed systematic approach to utilizing LIDAR Data to analyze roof structures in buildings. Several studies on generating 3D buildings have worked on similar workflows to achieve desired outputs. This workflow of working with LIDAR is divided into phases, from data cleaning to analyzing the processed data.

4.4.1 Preprocessing LIDAR Data

This includes noise removal and reclassification of point clouds to the respective categories such as Building, Vegetation, and ground points, hence preparing the data to be processed for a given area of interest. (El-Ashmawy and Shaker, 2014). This step ensures that the data is clean and accurately represents the built environment and terrain.

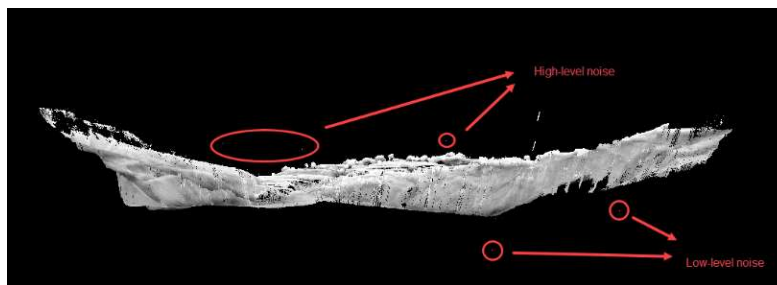


Figure 22 Noise from Point Cloud

4.4.2 Generating Building Footprint

This step is crucial in generating 3D buildings, as it provides the building footprint from the terrain, establishing the spatial location of the building on which shading analysis would be performed. (Latif et al., 2012). The building footprint is extracted from the processed LIDAR data by filtering the Building Class Point Clouds and populating them as a raster. This process converts the populated raster to a polygon and eliminates polygons based on area and noise.

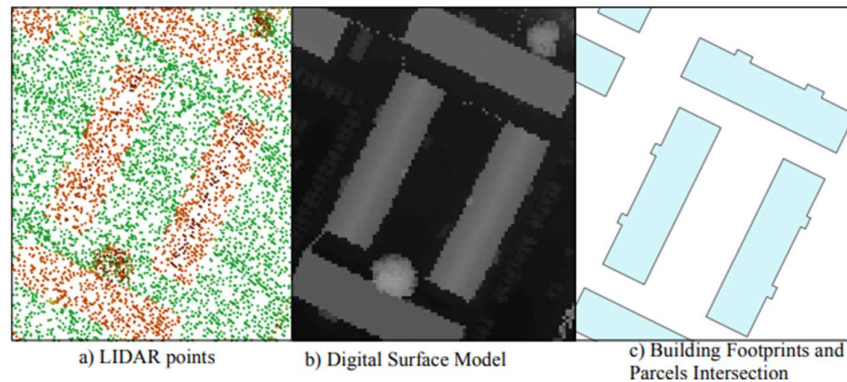


Figure 23 Generating building footprint from LIDAR (Boz et al., 2015)

4.4.3 Generating 3D Building Multipatch:

3D Building provides a realistic representation of building rooflines, crucial for accurate shading analysis. The process would start by extracting the ground elevation from the LIDAR data, forming DSM and DTM rasters. The normalized DSM is calculated

$$nDSM = DSM - DTM$$

A 3D model is created by extruding the building footprint to the LIDAR height of the respective Building. A study from (Jayaraj and Ramiya, 2018) showed potential approaches for generating LOD1, LOD2, and LOD3-based 3D Buildings from LIDAR. The process would utilize DSM, DTM, and nDSM raster to estimate the Base height and Eave Height of the 3D Buildings; considering the use of a single software approach, the 3D Basemap solutions from ArcGIS Pro would be a potential tool to generate and extrude 3D Builds from the building footprint. The figure below shows the comparison of the LOD2 model generated from ArcGIS Pro and Opensource Software; it is observed that the Level of Detail generated from ArcGIS Pro would be essential for the accurate generation of 3D Buildings for better shadow estimation.

The underperformance of PV Systems on the DC Side

Understanding shading Effects in PV Systems using LIDAR

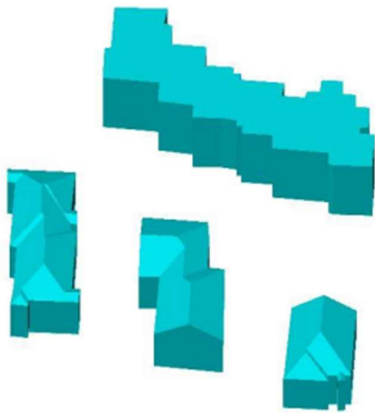


Figure 24 LOD2 3D Buildings generated from 3D Basemaps in ArcGIS (Jayaraj and Ramiya, 2018)



Figure 25 LOD2 3D Buildings generated from Open Source Software (Jayaraj and Ramiya, 2018)

4.4.4 Preparing and Performing Shading Impact Analysis on 3D Buildings

Shading Impact Analysis involves simulating the sun's movement across the sky and observing its interaction with the 3D Building Models and the respective rooflines over time. This could be performed using a Development Impact Analysis, a proprietary tool from ArcGIS that allows detailed solar radiation and shadow analysis across different times of the year. The tool uses other sub-tools like Create Sunpath to calculate the solar azimuth and elevation of the sun across the sky for a given day and year (fig) and Generate shadow panels based on the sun's position and shading impact on the buildings (fig)

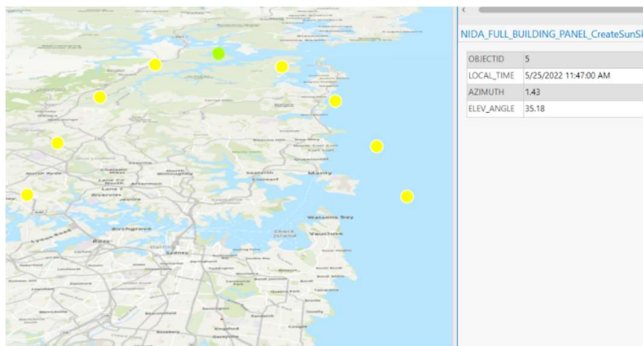


Figure 26 Sunpath Generator Tool in ArcGIS

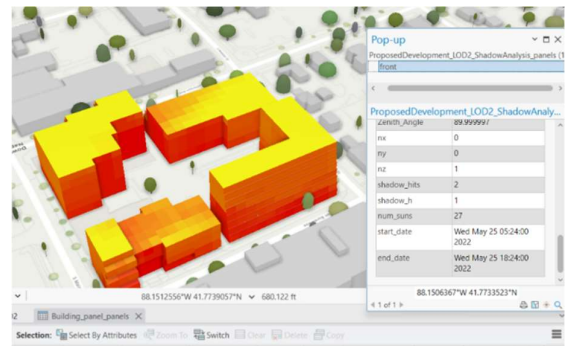


Figure 27 Illustration of Shadow impact Analysis in ArcGIS

4.4.5 Identify Shaded String

The specific PV Strings potentially impacted by the shading are identified by overlaying the shading analysis results on the actual roof imagery to determine the roof and PV location. The PV Schematics data would help identify the shaded string and would help further funnel down the analysis to the specific PV String. This process would involve georeferencing a GEOSAT image onto the spatial coordinate (with Latitude and Longitude), where High-definition satellite imagery of the building would be exported with

The underperformance of PV Systems on the DC Side

Understanding shading Effects in PV Systems using LIDAR

geospatial referencing (Herbei et al., 2010) . It would be used to form an overlay image on the actual rooftop mapped to the LIDAR coordinates.

The further process of PV String Identification would involve the formation of PV Module Polygons through Imagery shading. Comparing the shadow analysis with the PV module layout and the PV schematics would indicate the shaded string to be modelled.

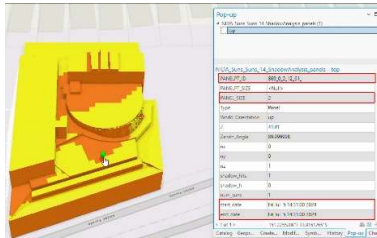


Figure 28 Shadow Impact Analysis of NIDA on Jul,5 02:31PM

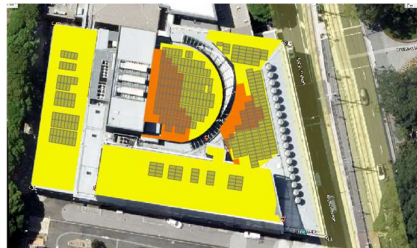


Figure 29 Shadow Panels overlapped with PV Panel Polygons

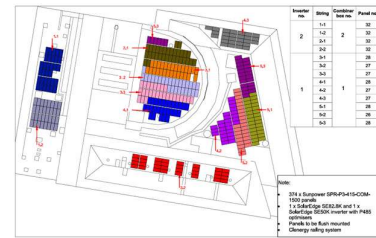


Figure 30 PV Schematics of NIDA

4.4.6 Generating Shading Profile

This process would concentrate on the shading profile of a specific string across the day on a 5m interval to ensure that minute changes in shading patterns were recorded in the shading profile. The process would involve using a 2D DSM raster and a Hill shade analysis on the specific string to quantify the degree of shading across the day. Using Hill Shade analysis to determine the shading profile increases the study's sensitivity to as low as 0.5m. This is visualized in Fig 31-32

The raster would be put through several filtering processes to identify specific regions of complete shading. This would involve smoothing Filters to reclassify the raster from 0-255 to (1-5/8). Considering a 5-minute observation frequency, this process would be implemented on a ModelBuilder in a looped environment. (Appendix B.5)

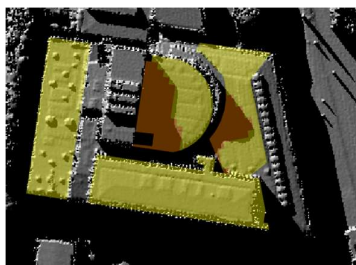


Figure 31 Shadow Panels overlapped on Hillshade Analysis Layer

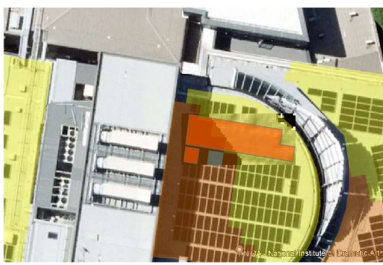


Figure 32 PV String Layout overlapped on Shadow Panel and Hillshade Analysis Layer

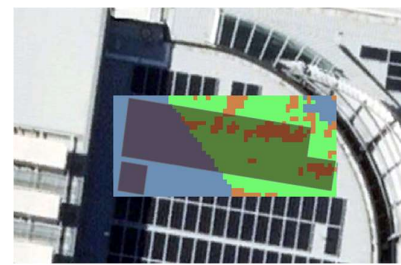


Figure 33 Reclassified layer output from the model

The output from the process would be a CSV file containing the Zonal statistics of the raster and histogram data of the share (Count) of pixel value on the PV String. From the above fig, a Hillshade

raster which has 0-255 is cut down and reclassified to 0-3 by forming Intervals based on the 2nd Standard Deviation Limits from the Upper and Lower value of the Clipped Hilshade Pixel from Figure 33.

4.5 Modelling in Python:

After identifying the shaded string, the selected PV string configuration would be modelled onto Python via PVLIB. The PV schematic data would be used to get information on the PV system's azimuth and tilt orientation. The schematics also provide details about the PV Panel and Inverter used in the system. The PV string configuration is required for accurate system modelling.

4.5.1 Modelling Plane of Irradiance

Initially, the PV String is modelled based on input from clear_sky values. The plane of the array is calculated for the clear_sky values and plotted to identify the maximum power generated from the string. After successful modelling, the weather data is obtained to calculate the string's POA and the respective DC Power is calculated based on POA_global. It is plotted to ensure the simulated max DC Output Power is within the range of the string's actual DC Power.

To calculate the solar irradiance on the plane of the array, the Solar Zenith and Azimuth angles are calculated relative to the location, orientation, and day of observation on the panel. The solar Zenith and Azimuth

$$\theta_z = \arccos(\sin(\phi) \times \sin(\delta) + \cos(\phi) \times \cos(\delta) \times \cos(h))$$
$$\gamma_s = \text{atan2}\left(\frac{-\sin(h)}{(\cos(h) \times \sin(\phi) - \tan(\delta) \times \cos(\phi))}\right)$$

(Reda and Andreas, 2008)

The Solar azimuth and zenith is calculated through pvlib pvlib.solarposition.get_solarposition(latitude, longitude), and it returns azimuth and zenith based on the time period of weather data

The angle of sun's rays to the panel (θ) is calculated as

$$\theta = \cos(\sin(\delta) \times \sin(\phi) \times \cos(\beta) - \sin(\delta) \times \cos(\phi) \times \sin(\beta) \times \cos(\gamma) + \cos(\delta) \times \cos(\phi) \times \cos(\omega) \times \cos(\beta) + \cos(\delta) \times \sin(\phi) \times \cos(\omega) \times \sin(\beta) \times \cos(\gamma) + \cos(\delta) \times \sin(\omega) \times \sin(\beta) \times \sin(\gamma))^{-1}$$

δ is the solar declination angle.

ϕ is the latitude.

β is the tilt angle of the panel.

γ is the azimuth angle.

ω is the hour angle.

The POA_unshaded [Global] is calculated from

$$POA_unshaded[Direct] = DNI \times \cos(\theta)$$

$$POA_unshaded[Diffuse] = DHI \times TF \text{ (Transposition Factor)}$$

By default, pvlib considers the Hay-Davies Transposition Factor, where the model assumes a uniform distribution of the diffuse sky radiation.

$$\text{Where } TF = F_{Hay} = \left(1 - \frac{DNI}{GHI}\right) \times \left(\frac{1 + \cos(\beta)}{2}\right) + \frac{DNI}{GHI} \times \frac{\cos(\theta)}{\cos(\theta_z)} + \text{Ground Reflectance Term}$$

(Nassar et al., 2020)

$$POA_unshaded[Ground] = GHI \times \rho \times ((1 - \cos(\beta))/2)$$

$$POA_unshaded[Global] = POA_unshaded[Direct] + POA_unshaded[Diffuse] + POA_unshaded[Ground].$$

(F. Holmgren et al., 2018)

The POA in pvlib is calculated via pvlib.irradiance.get_total_irradiance() with passing GHI, DHI, and DNI from weather data, and the calculated Solar azimuth and zenith values as the function parameters to compute solar irradiance on the POA. The default HayDavies Model is used for POA calculation in pvlib.

4.5.2 Modelling Shaded_POA:

Form the exported .csv file from the previous process of estimating the string's shading profile. The shading percentage for the string is calculated over a 5m period. The area under shading is assessed by identifying the Lowest Pixel from the reclassified raster, which denotes the Zero Pixel from the Hillshade raster. (Zhao et al., 2021)

$$\text{Shading (\%)} \text{ on the PV String} = \frac{\text{Count (Pixel Value = 1 from Reclassified Zonal Table)}}{\text{Total Count of Pixels on the string}}$$

The Plane of Irradiance of the shaded String is calculated in Python based on the actual meteorological weather data and is calculated by

$$POA_shaded[Direct] = POA_unshaded[Direct] \times \text{Shading Factor}^*$$

$$POA_shaded[Direct] = POA_unshaded[Direct] \times (1 - \text{Shading(\%)} \text{ on the PV String})$$

$$\begin{aligned} POA \text{ on Shaded Array} = POA_shaded[Global] &= POA_shaded[Direct] \\ &+ POA_unshaded[Diffuse] \end{aligned}$$

(Miranda et al., 2021)

*Where SF =0 (no Sunlight on string) when 100% Shading on the string and vice versa

4.5.3 Modelling DC Power Output

The DC Power output from PV is calculated by considering the POA irradiance, the characteristics of the PV Module, and the environmental conditions, such as temperature and wind speed.

The **SAPM temperature model** calculates cell temperature. It is best suited for systems where NOCT and wind speed data for the module are available and is modelled to get accurate PV output. Since the PV module on the chosen site location is Suntech Power Pluto 215Udm is a monofacial panel hence the TEMPERATURE_MODEL_PARAMETERS would be modelled for glass/polymer module

Where

$$T_{Module} = E \times \exp(a + b \times WS) + T_a$$

(F. Holmgren et al., 2018)

Where

- T_a is the ambient temperature in degrees Celsius.
- E_{POA} is the Plane of Array (POA) irradiance in W/m².
- WS is the windspeed at 10m

Temperature Model parameters are used to model the impact of temperature variation on DC output. The air temperature and wind speed of 10m is utilized to compute the cell's temperature, which would affect the panel's DC Power output.

The PVwatts DC Power Models compute DC Power output from the string. Environmental Parameters such as POA[Global] and Cell Temperature are passed along with P_{dc}, Power from the PV Module from STC, and the module's power coefficient.

$$P_{DC} = \left(\frac{G_{POAEFF}}{1000}\right) \times P_{DC0} (1 + \gamma_{pdc} (T_{Cell} - T_{ref}))$$

(F. Holmgren et al., 2018)

Where

G_{POAEFF} = POA_ Effective Global Irradiance

P_{DC0} = DC Nameplate

γ_{pdc} = Temperature Coefficient for Power

T_{ref} = Cell reference Temperature = 25°

Other models, such as SAPM, were not used in the computation of DC Power because there was a lack of data on the module's SAPM coefficients. The graphs are plotted and then analyzed to identify the patterns in the findings.

4.6 Tools Used in the Workflow

This section will compare the available tools for the requirements of our study; a comparison is made for two primary components of the study: 1. Geographic Information Software and 2. Modelling in Python

4.6.1 Geographic Information Software (GIS):

Considering using LIDAR for the study, the two potential Geographic Information Software proposals were ArcGIS Pro from ESRI and QGIS from Gary Sherman. However, ArcGIS Pro was chosen for the study to compare the possible tools for processing LIDAR and the ease of implementing the computation of LIDAR. The table below shows the comparison study between ArcGIS Pro and QGIS for the tasks to be completed for the study.

S.no	Task	ArcGIS	QGIS	Comparison
1.	Preprocessing LIDAR Data	Tools: Integrated LIDAR Processing tools with classification and noise removal	Tools: Plugins like LAS Tools are required for LIDAR data processing, which are less integrated.	ArcGIS offers a more friendly, seamless, user-friendly LIDAR processing experience, while QGIS requires additional setup and plugins.
		Ease of Use: Intuitive interface with comprehensive tools for filtering and classifying data.	Ease of Use: Effective but requires familiarity with plugins, which can be complex to set up.	ArcGIS provides a more integrated environment, reducing the learning curve compared to QGIS.
2.	Generating Building Footprint	Tools: Easily extract building footprints using the built-in LIDAR processing and geoprocessing tools.	Tools: Footprint extraction is possible through plugins but could be more streamlined.	ArcGIS offers more direct and integrated tools for footprint generation, making the process faster and more efficient.
		Ease of Use: Direct access to tools within the same platform, simplifying workflow.	Ease of Use: Requires additional plugins and more manual steps, increasing complexity.	ArcGIS's built-in tools simplify the process, while QGIS users need to manage multiple plugins.

3.	Generating 3D Building Multipatch	Tools: The 3D Basemap solution in ArcGIS provides robust tools for generating 3D multipatch models. ArcGIS can also support City Engine 3D Rule packages to generate LOD2 Buildings.	Tools: Basic 3D visualization through QGIS 3D plugin, with limited multipatch support.	ArcGIS's 3D Basemap solution is far superior for generating detailed 3D building models compared to QGIS.
		Ease of Use: Integrated workflow for creating and editing multipatch models.	Ease of Use: Requires advanced skills and additional plugins for similar tasks.	ArcGIS provides a more user-friendly and comprehensive 3D modelling environment.
4.	Preparing and Performing Shading Impact Analysis	Tools: Development Impact Analysis solution in ArcGIS, designed explicitly for shadow and shading analysis.	Tools: Basic shading analysis can be performed but requires plugins like QGIS2ThreeJS or additional scripting	ArcGIS offers a specialized solution for shading analysis, whereas QGIS's capabilities are limited and require more effort.
		Ease of Use: User-friendly, integrated tools with detailed reporting and analysis capabilities.	Ease of Use: It is a more manual process, less intuitive, and requires more profound knowledge of plugins.	ArcGIS's dedicated tools for shading analysis provide a much easier and more effective solution than what is available in QGIS.

Table 3 Comparison of GIS Software

4.6.2 Modelling PV System

When selecting an Integrated Development Environment (IDE) for modelling in PV system analysis, particularly for tasks such as handling high-resolution meteorological data and conducting shading performance analysis, it's essential to consider the specific features, usability, and tools each IDE offers. The table below discusses the comparison of various IDE.

S.No	Criteria	Spyder	PyCharm	Jupyter
	Data Handling & Visualization	Integrated Variable Explorer for real-time data inspection is ideal for handling and visualizing large datasets like 5-minute meteorological data.	Strong data handling capabilities but lacks built-in real-time data inspection features, requiring plugins or additional setup.	Excellent for interactive data exploration and visualization but less suited for complex, multi-file projects.

	Integration with Libraries	Seamless integration with PVlib, SciPy, and Matplotlib makes it straightforward to set up and use for PV system modelling.	It supports integration with scientific libraries but may require additional configuration and lacks the native support that Spyder offers.	It is well-suited for using scientific libraries interactively but needs more than the full IDE capabilities needed for large-scale modelling.
	Debugging & Error Handling	Robust debugging tools with an intuitive interface, including real-time error highlighting and step-through debugging.	Advanced debugging features with extensive support for complex projects, but the interface may be overwhelming for scientific tasks.	Limited debugging capabilities, focused more on code execution and visualization than comprehensive debugging.
	Learning Curve	There is a low learning curve for those familiar with scientific computing, especially users transitioning from MATLAB.	A steeper learning curve exists, especially for users without a software development background.	Minimal learning curve for interactive coding and visualization but not designed for complex project development.

Table 4 Comparison of Python IDE

Various specialized tools are employed in the workflow to ensure accuracy, efficiency, and comprehensive analysis. Each tool is crucial in different workflow stages, from data acquisition and preprocessing to final shading estimations and visualization. The table below shows the tools under various software utilized from the preprocessing stage until Validation and Calibration.

S.No	Software	Tools/Library	GeoProcessing Tools / Functions
1.	ArcGIS	Conversion Tools	LAS Dataset to Raster Raster to Polygon
		3D Analyst Tools	Slope Aspect LAS Building Multipatch Classify LAS Noise Extract LAS Regularize Building Footpath
		Spatial Analytics	Majority Filter Hillshade Analysis Solar Radiation Raster
		Image Analyst Tools	Focal Statistics Georeferencing
		Data Management Tools	Create LAS Dataset Zonal Statistics as Table LAS Dataset as Statistics Eliminate Polygon Part
		3D Basemaps	Extract Elevation from the LAS Dataset Roof Segmentation Tool Create 3D Buildings

The underperformance of PV Systems on the DC Side
 Understanding shading Effects in PV Systems using LIDAR

			Fuse Buildings
		Developmental Impact Analysis	Sunpath Tool Shadow Analysis Visualize Shadows
2.	Spyder IDE (Python Environment)	Pvlib	Location() Get_solarposition() irradiance.get_total_irradiance temperature.sapm_cell pvsystem.retrieve_sam pwwatts_dc
		Pandas	read_csv reindex .loc[]
		matplotlib	Plot()
3.	Tableau	Visualizer	

Table 5 Tools and functions used in the study

4.7 Workflow

This section explains the workflow of shading estimation, from preprocessing to estimations. Figure 34 below shows the sequential processes of generating 3D Buildings to perform shadow analysis.

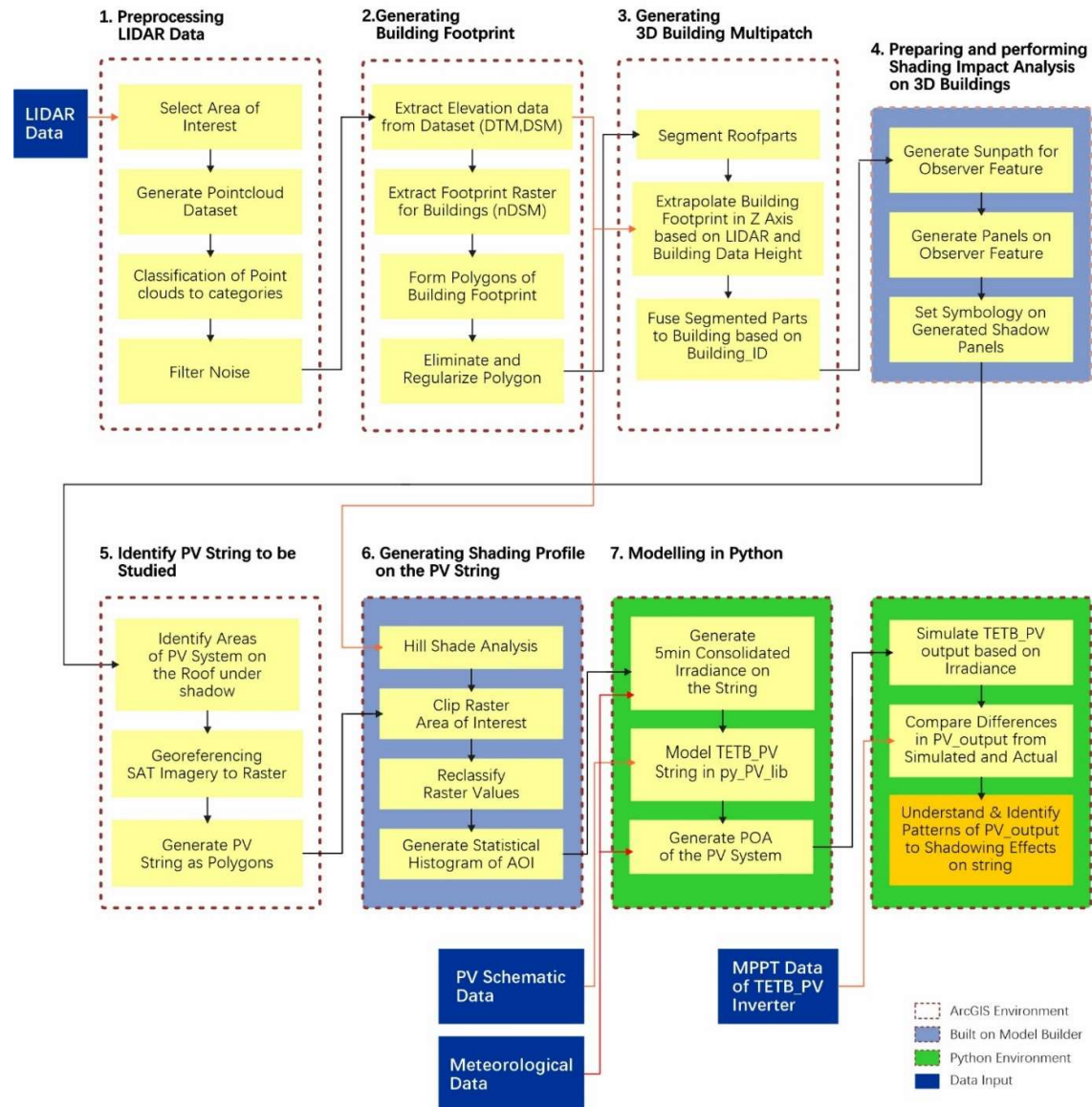


Figure 34 Detailed Workflow of the study

5. Results and Analysis

The section discusses the results and progress of preprocessing LIDAR to generate 3D Buildings and performing the Shadow Impact Analysis on the chosen location, TYREE Energy Technology Building (TETB) at (-33.9175, 151.2268).

5.1 Preprocessing LIDAR Data:

5.1.1 Select Area of Interest

The LIDAR data from ELVIS was available in batches of 4.5 km². As the area of interest had been chosen from the previous section, the LiDAR data available in the form of LAS extension about the given area of interest is Extracted through the Extract LAS Tool since the site selection for the study is Tyree Energy Technology Building (TETB), the location of interest also considers nearby building in the proximity to understand the effect of shading right from sunrise to sunset.

The initial step mandates ensuring all elements of the map/Scene follow spatial reference XY: GDA2020 MGA Zone 56 and Z: AHD. The standard unit of measurement in this study is meters.

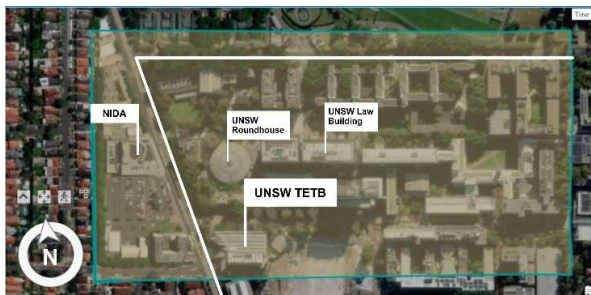


Figure 35 Area of Interest for the study

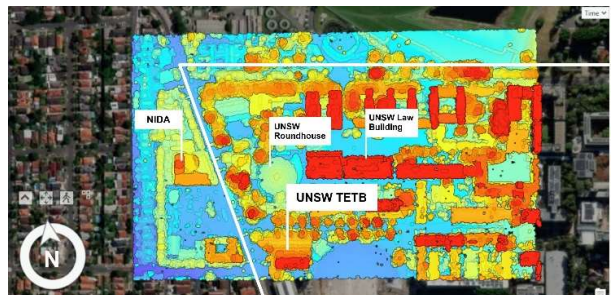


Figure 36 LIDAR clipped to Area of Interest

5.1.2 Classification of Point Clouds:

The classification of point clouds allows for the identification and separation of various surface types, such as ground, vegetation, buildings, and other structures. Ensuring proper segmentation is mandatory when defining the edges and dimensions of any subject on the LIDAR Map, as it is essential for analyzing specific features that impact shading. This would improve the Terrain and Surface raster generated post-cleaning.

Figure 37 shows classified LIDAR data with few errors in classification, which could lead to misinterpretation of the point cloud and wrong estimation and dimension.

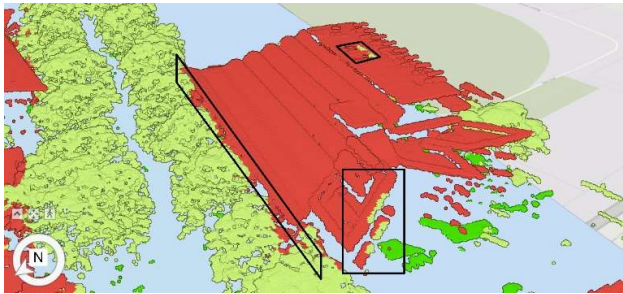


Figure 37 Point Clouds with Noise and Irregularities

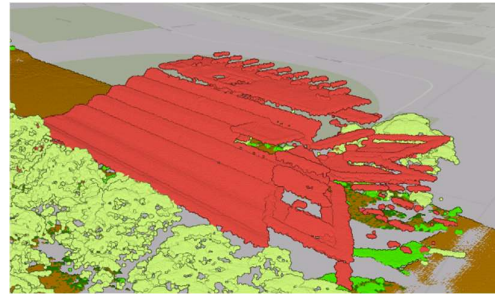


Figure 38 Preprocessed LAS Dataset with point cloud reclassification.

Of the roof. Hence, point clouds are manually classified to recategorize High vegetation point clouds with the building point clouds and vice versa, as seen in Figure 38.

5.1.3 Filter Noise:

Certain point clouds would be accounted for as Noise and High Noise based on the offset of their xy and z axes. Noise in LIDAR data would lead to incorrect classification, specifically in areas with low point density. Hence, the noise point clouds were identified and removed using the Classify Noise Tool by limiting the height extent of required point cloud data for further processing.

The filtered, reclassified, and preprocessed data is then converted to a LAS Dataset, efficiently stored in 3D (x,y,z) coordinates. Around 67199 points were removed within the Area of Interest from the source point cloud data, as noise and high noise, ranging from -19m to 97m in height. The creation and storage of the LAS Dataset are essential for further data processing related to the analysis.

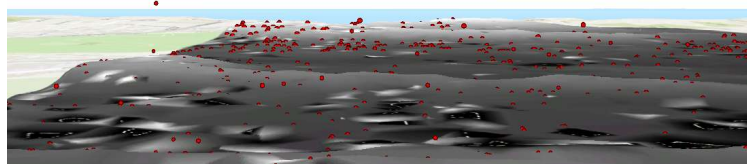


Figure 39 Noise Point Clouds within the Area of Interest

5.2 Generating Building Footprint:

The process involves 2D visualization of classified LAS Dataset, and elevation is extracted from the point clouds. The Digital Surface Map (DSM) raster is generated with building and ground point clouds, as shown in Figure 40, and the ground point cloud is used to create a Digital Elevation Map (DEM) raster Figure 41. A normalized DSM raster is generated by subtracting DSM and DEM to obtain normalized building height, as shown in Figure 42. Extract Elevation. To simplify the process, the Extract ground

elevation LAS Dataset Geoprocessing tool from the 3D Building Tool of ArcGIS is used to compute DSM, DTM, and nDSM of the raster of specified cell size.

An optimal cell size of 0.3 is used to maintain the raster's essential detail and smoothness for further processing. The generated rasters would be used to determine the height characteristics of components such as Facades, towers, and HVAC systems on the roof.



Figure 40 DSM Raster



Figure 41 DTM Raster

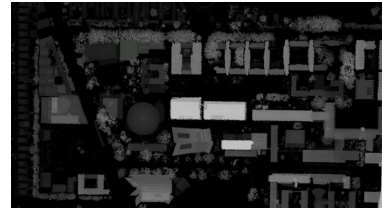


Figure 42 nDSM Raster

The LAS Dataset is filtered and processed through LAS Point Statistics as a Raster geo-processor from Data Tool Management to form a raster only with the point of buildings, as shown in Figure 43.

The raster formed in the process contains the filtered point clouds of buildings from the LAS dataset. This was then converted to a polygon through the Raster to Polygon Tool (Conversion Tools), as shown in Figure 44. This process converts the cell with the same value from a raster to a simple polygon with unique OBJECT_ID and Shape length and area attributes. The Eliminate Polygon tool removes minors and filters out the undesirable polygons on the raster. The regularized Building Footpath Tool fills the gaps between the gaps formed in the Raster to Polygon Tool.

Parameters such as Tolerance, Density, Precision, and Diagonal Penalty were set to 1,1,0.25 and 1.5 based on suitable optimization.



Figure 43 LAS Point as Statistics Tool



Figure 44 Raster to Polygon Process

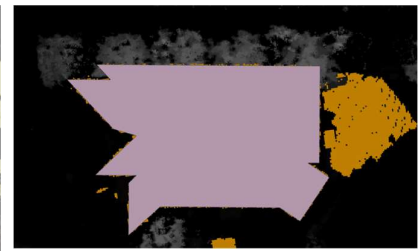


Figure 45 Regularized Building Footprint of TETB

Similarly, the footprint is obtained for other buildings near the TETB Building. The footprints of the UNSW Law Building, the June Griffith Building, NIDA, and the New College Postgraduate Village Building have been regularized for further processing to generate a 3D Building Multipatch. The footprint of the TETB Building and other neighboring buildings are shown in Figure 45.

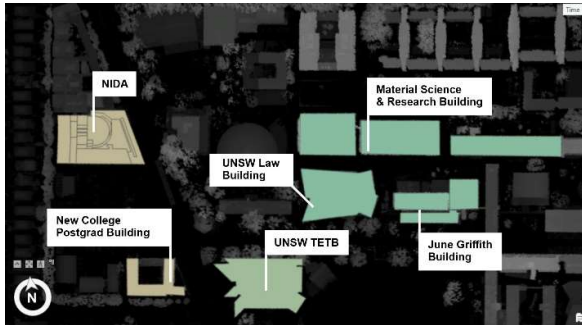


Figure 46 Regularized Building Footprint of Neighbouring Buildings around TETB

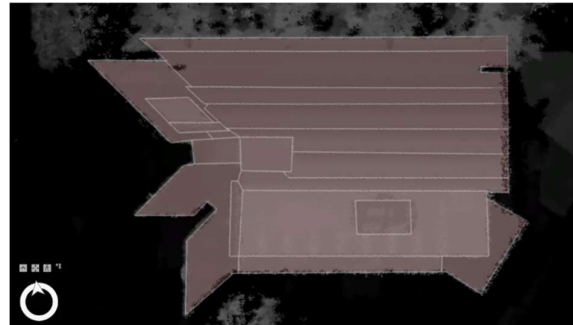


Figure 47 Segmented Rooflines of TETB

5.3 Generating 3D Building Multipatch :

5.3.1 Roof Segmentation

The first step in generating 3D base maps is manual/automated segmentation of roof parts. On initial analysis of the TETB roof's roof type, it was identified that the edges of the roof seem to have curved or angled overhangs to which the PV Power system is mounted. This leads to complicated generation of roof segmentation through an automated tool-based approach.

A manual rooftop segmentation approach is taken, especially for TETB, to segment the roof into various sections. This process employs feature class modification through split and edit Vertices Tools. The transparency of the polygons is reduced so that they can be seen through the DSM raster of the roof sections of the building for effective segmentation. The segmented Roof parts of TETB are shown in Fig. This segmentation separates roofs of various heights and uniquely distinguishes small tower structures on the building on a 2D raster.

5.3.2 Extrude Building in Z-Axis to Create 3D Shapes:

This process utilizes a 3D Basemap tool (Create 3D Buildings) where the input for the geoprocessing involves the feature class of segmented roofs and elevation rasters that include DSM, DTM, and nDSM. The toolset is part of the ArcGIS Pro. It leverages the capabilities to generate 3D environments, where it calculates the base elevation and the Eave Height of a roof from the Raster data. The tool classifies the roof type into four types (Flat, Gable, Shed, and Hip). This classification is primarily done by estimating the height and eave height of the roof; the segmentation data is utilized to identify individual objects in a building and extrude them as 3D objects based on elevation data. A confidence measurement is

performed against the 3D Building Roof Forms and the DSM raster of the building to ensure accurate segmentation.

The symbology is changed to obtain 3D Buildings (polygons). The polygons are fused to form buildings based on the Building_ID attribute, and the Level of Detail 2 (LOD2) rule package from CityEngine is used to generate extrapolation of 3D structures.

Figure 48 below shows the 3D building formation of TETB (primary location). The neighboring buildings, including NIDA, UNSW Law Building, June Griffith Building, and New College Postgraduate Buildings, are shown in Figure 50.

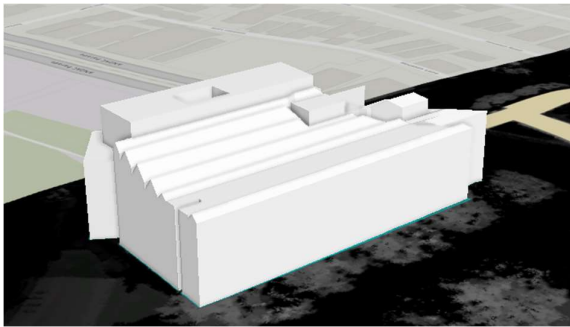


Figure 48 3D Multipatch of TETB



Figure 49 Google Earth 3D Model of TETB

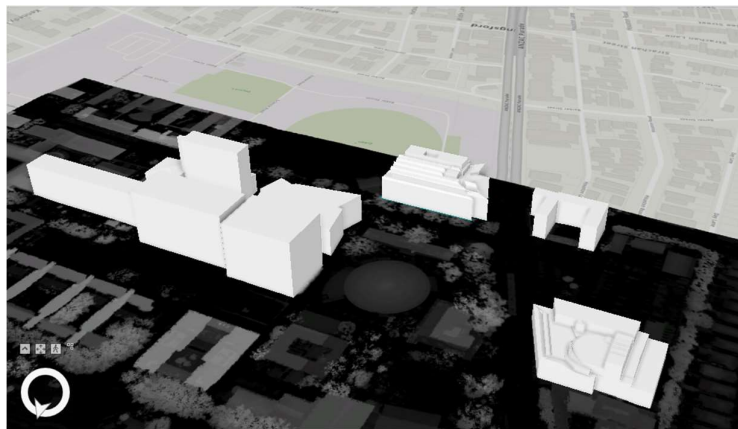


Figure 50 3D Multipatch of Neighbour Buildings around TETB

5.4 Shading Impact Analysis

To perform a shadow impact analysis over a 30-minute period, a Model Builder System is implemented in ArcGIS using Shadow Impact Analysis Geoprocessor Tools from the Development Impact Analysis Solution of ArcGIS. The suns shown in Fig and Fig represent the positions of the Sun Generated with

respect to the TETB Building. Fig compares the position of suns in December (Yellow Suns) and June (orange Suns)



Figure 51 Sun positions on 21/12/2021

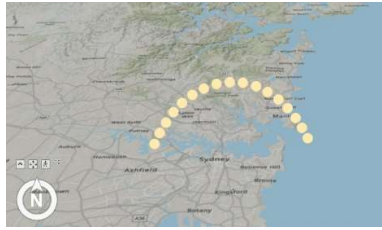


Figure 52 Sun positions on 25/06/2021

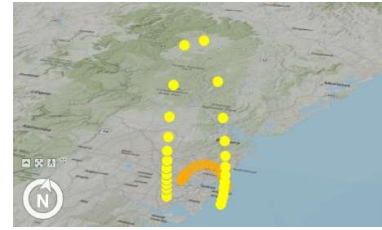


Figure 53 Comparison of Sun position for July and December

The individual positions of the Sun are fed as input to the Shadow Analysis Geoprocessor, and the shadow panels on TETB are computed for the date of 21st December 2021. Figure 54 below shows the shadow panels during the start and end hours of the day to understand the shaded regions on the roof.

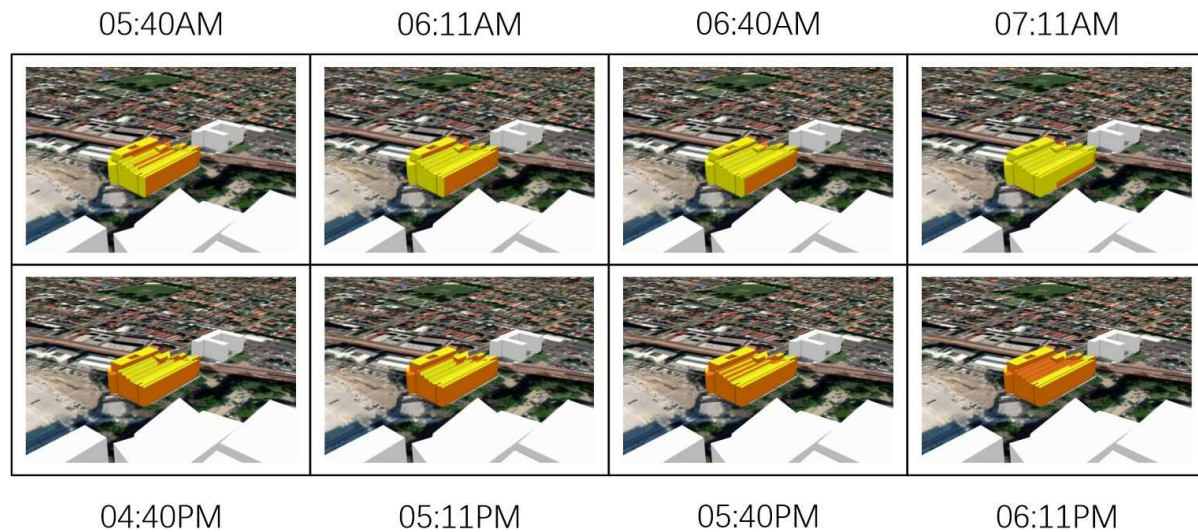


Figure 54 Shadow Impact Analysis on TETB 3D Building on the first and last hours of 21/12/2021

5.5 Identify Areas of PV System on the Roof under Shadow

The previous process would lead to the identification of the shaded string of the PV Solar Plant on a 3D Building. However, due to the high tilt angles of the PV system on certain Roofs of the TETB building, overlapping the PV panels on the 2D map of the shadow panels was challenging. Observations from the previous process, correlating with the position of the PV System on the PV Schematics, show that string 7C is undergoing shading in December and June. Upon performing the Hill shade analysis of the DSM raster obtained previously, Figure 55 showed shadows that overlapped the 3D shadow panels.

Georeferencing the High-Res Satellite Image is performed with 6 points reference with the DSM raster from LIDAR, and the polygon panels are formed as shown in Figure 56. The superimposed images of the

panel with the Shadow Panels obtained from the shadow analysis and comparing them with the PV Schematics of TETB revealed that PV String 7C (as seen in Figure 57) is a potential system to be studied as the system underwent significant shading as observed on Dec 21st, 2021, at 03:45 PM shadow analysis and hillside analysis. The PV Schematics of TETB are attached in the Appendix A.

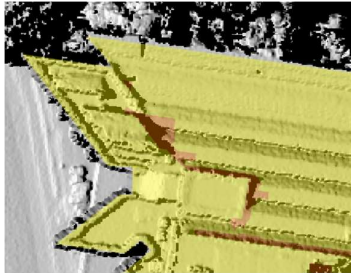


Figure 55 Shadow Panels of TETB superimposed on Hillshade Analysis



Figure 56 TETB Imagery Georeferenced and PV Polygons on Roof

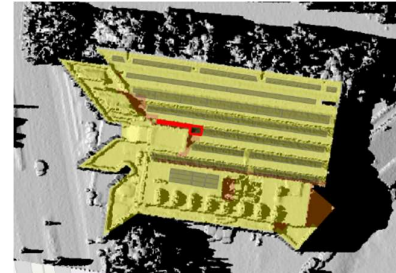


Figure 57 PV String 7C Shaded.

5.6 Estimation of Shading Profile on the String

The shading profile also had to be estimated to analyze 5 minutes of DC Power from the PV String. The solar azimuth and elevation are generated as a CSV for a given day using the pvlib Library in Python (Appendix B.4), as shown in Figure 58. They are provided as input for Hillshade analysis, where the hillshade analysis enables the shadow modelling feature on the raster. A ModelBuilder in ArcGIS Pro is utilized to form a workflow using Hillshade Analysis Generation from the DSM created in Section 5.2. The Model Builder was built on the process involving, as shown in Appendix B.2 ,

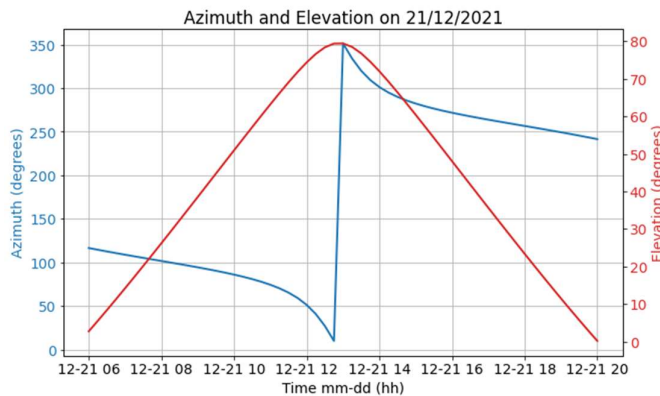


Figure 58 Azimuth and Elevation for 21/12/2021

Hillshade Analysis > Clipped on the New Area of Interest (PV String 7C) > Majority Filter > Raster Reclassification > Majority Filter > Zonal Statistics as a Table> CSV Export

This process ensures that the integer value from Hillshade Analysis, which usually ranges from 0 to 255 in pixel value, is reclassified to a lower 1-5 / 1-8 based on the range of the Min and Max limit on a clipped raster at a given time frame. Figure 59 below shows the raster's sequential change from Hillshade

Analysis to the final Reclassified Raster for the final hours on 21st December 2021.

The final reclassified Raster is put through a majority filter to make sure the shaded pixels (1) are populated by checking on four other neighbour pixels; this is to ensure that only the sharp contour of the projected shading is captured on the raster. The final raster is converted to a table using Zonal Statistics as a Table Tool. The final table is converted to CSV, each file containing the pixel value and their respective count for 5 minutes across the day.

The underperformance of PV Systems on the DC Side

Understanding shading Effects in PV Systems using LIDAR

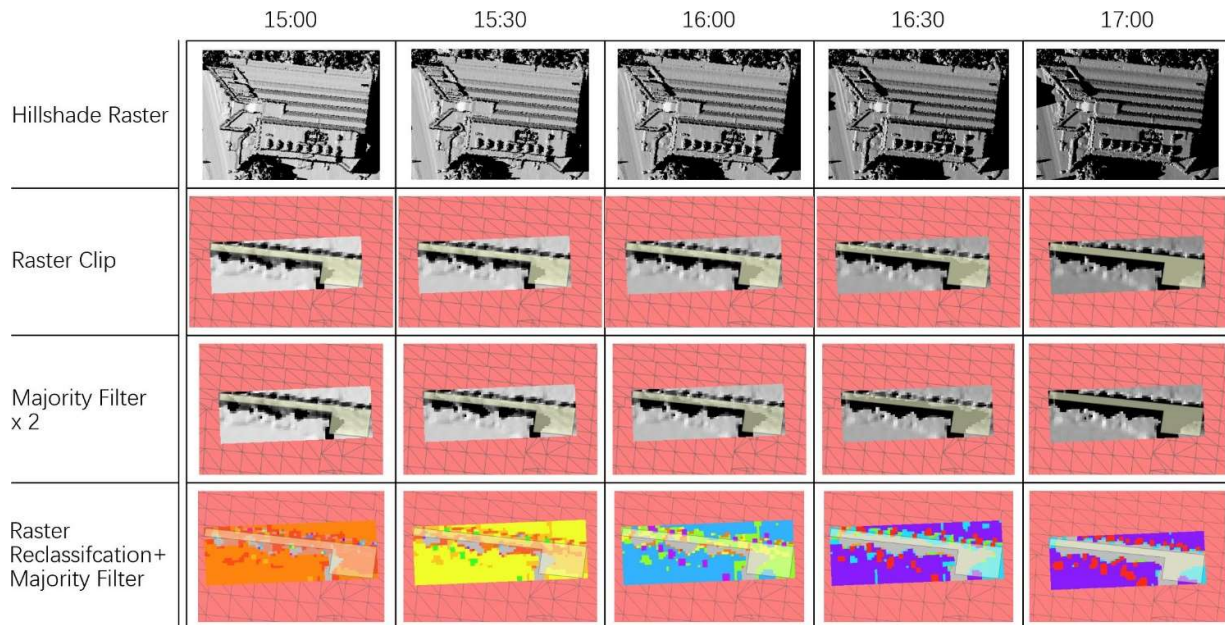


Figure 59 PV String Shade Analysis with ModelBuilder in ArcGIS

From 15:00hrs to 17:00hrs, a gradual shadowing effect was observed on PV String 7C, and a reclassified raster was formed to estimate the shading profile of the Inverter tower on the string.

5.7 Modelling in Python

The previous process generated around 171.csv files of 5-minute zonal data. A Python code (Appendix B.4) was written to consolidate the shading profile of the PV String by timestamp. As discussed in the previous section, 4.6.2, the string's shading factor is determined for the given day, and the plot of the shading percentage for 21st December 2021 is shown in Figure 60.

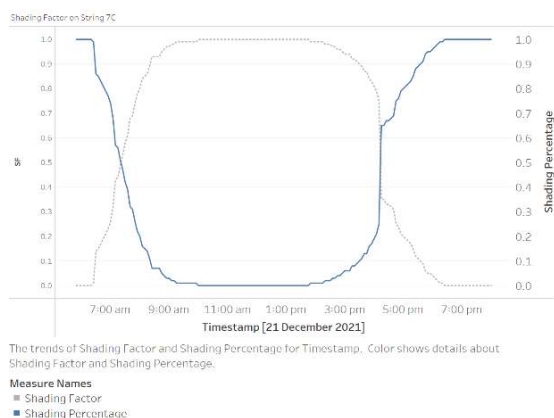


Figure 60 Shading Percentage vs Shading Factor on 21/12/2021

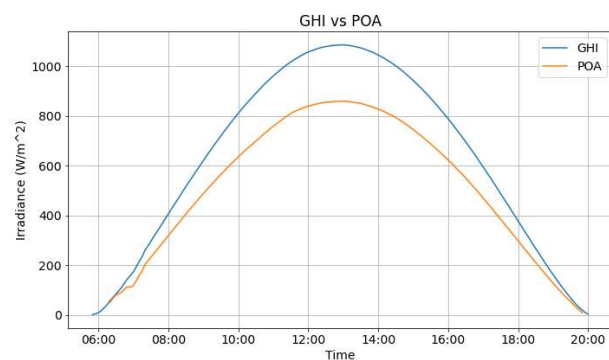


Figure 61 GHI vs. Calculated Plane of Array on 21/12/2021

The PV Schematics in Appendix A are used to model the PV System in Python (Appendix B.3). Considering the independent performance of the Sunny Boy Tripower Inverters, Python code is used to model MPPT

B of the system configuration, to which string 7C is connected. The solar azimuth and zenith are calculated through pvlib, passing the location's latitude and longitudinal parameters.

Meteorological data such as GHI, DNI, and DHI, along with the orientation of the modules from PV Schematics, are used to compute the plane of array irradiance. The default Hays-Davies Model is used to model the Diffused component of the POA. Figure 61 shows the plot of GHI vs. POA for 21 December 2021.

For the computation of DC Power, the cell temperature for the day is computed through the SAPM Model, as discussed in the previous section 4.6.2, where the shaded_POA[global] is passed as the irradiance, and the cell temperature is computed from the SAPM model considering the model type from the PV Schematics; the Panel Model Suntech Power Pluto 215W UDM is a monofacial module and is modelled as glass/polymer is used as inputs for the function pvlib.pvsystem.pvwatts_dc. The figure below shows the Shaded vs Unshaded plot of the Plane of Array Irradiance and the respective DC Output.

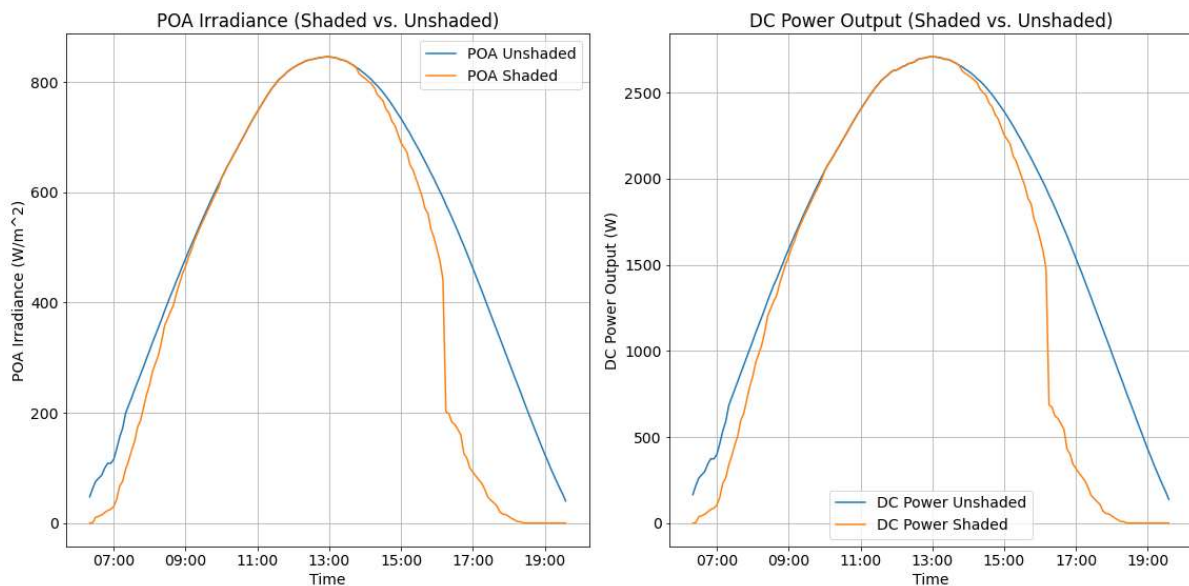


Figure 62 a) POA Shaded vs POA Unshaded. b) Shaded DC Power vs Unshaded DC Power from the string

As seen from the plotted graph, on comparing the POA_shaded vs. Unshaded POA, the impact of shading is observed to be impacted at 16:00hrs, and the shaded DC Power output follows a similar trend to that of the shaded POA incident on the PV String. The plot of the DC-shaded output shows the impact of shading on the string.

5.8 Result Analysis and Discussion

The DC output for the shaded and unshaded POA is plotted in Figure, and the string's DC Power Output, combined with other weather parameters like Air Temperature, windspeed_10 m, GHI, DNI, and GHI, is exported to be further visualized on Tableau with the actual inverter Data.

Tableau is used to visualize and compare the actual inverter parameters with the simulated parameters. The plot below shows the simulated DC Power Output vs. the Actual DC Power Output. The Inverter 7 Data, Simulated PV Data, and shading profile data are connected in Tableau through a Date Timestamp, and the output is visualized.

The Plot in the figure 63. shows the simulated vs. Actual DC Power vs. the shading percentage of the PV String. As observed from the graph, from 07:00 AM, as the shading percentage on the string decreases, the Output power from the Actual and the Simulated PV String also increases. At

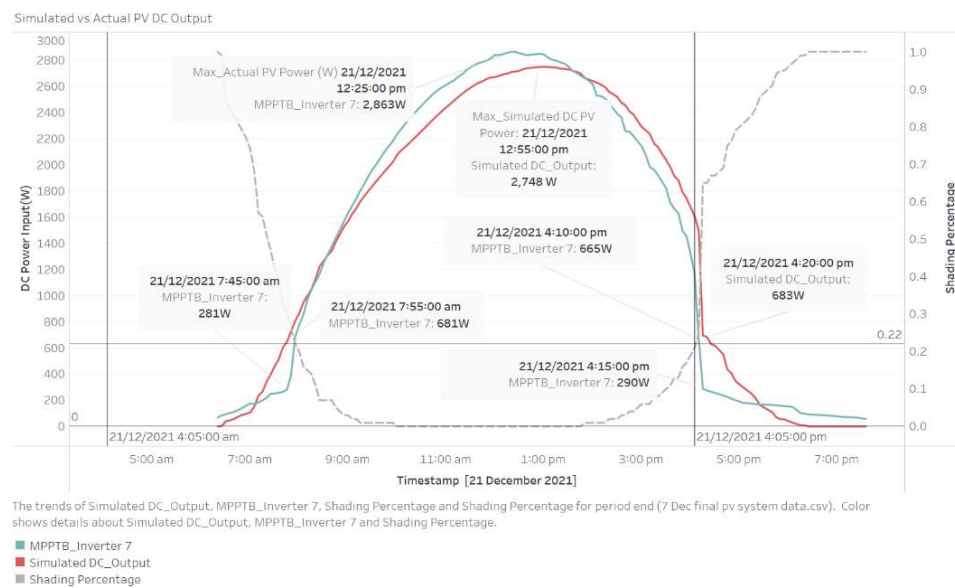


Figure 63 Simulated vs Actual PV Panel DC Output from String 7C with Shading Percentage

04:15 PM, a sharp increase in shading is seen due to the shading caused by the tower on the roof of TETB, resulting in a rise of 25% to 65%, leading to a sudden drop in PV string power (DC) from 449.9W to 205.4W to the inverter. A slight deviation in the Simulated vs. actual power profile has been observed, as there would be a subtle change in the degradation factor mismatch and assumptions, considering the adaptation of the model used in modelling temperature and irradiance on the POA. The module lacks the Sandia parameters, making it impossible to work on other models for POA irradiance calculations and testing with other DC Power modelling functions.

The underperformance of PV Systems on the DC Side

Understanding shading Effects in PV Systems using LIDAR

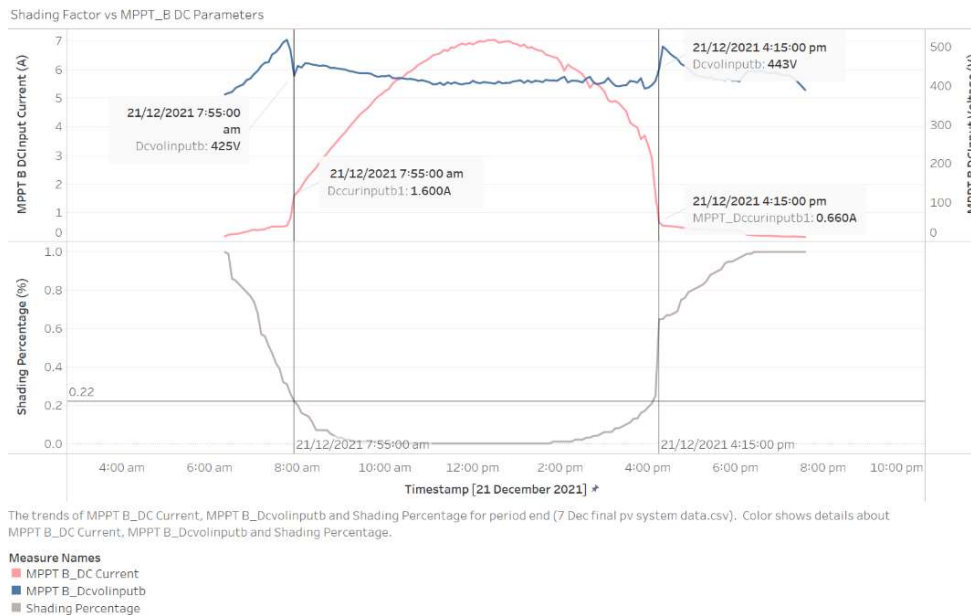


Figure 64 DC Current and Voltage from String 7C to Inverter vs Modelled Shading Percentage

string ramps up, the current output from the string ramps down due to shading from the tower's roofline. As the DNI component is cut due to shadowing, The current from the PV String persists in being generated due to the Diffuse component of the Plane of Array Irradiance. Also, it was observed that from 2:00 PM, as the shading percentage increases gradually from 0% to 20%, a ripple on the decreasing trend of the current and increasing trend of voltage is observed as the effect of bypass diodes shutting down parts of the PV module in the string.

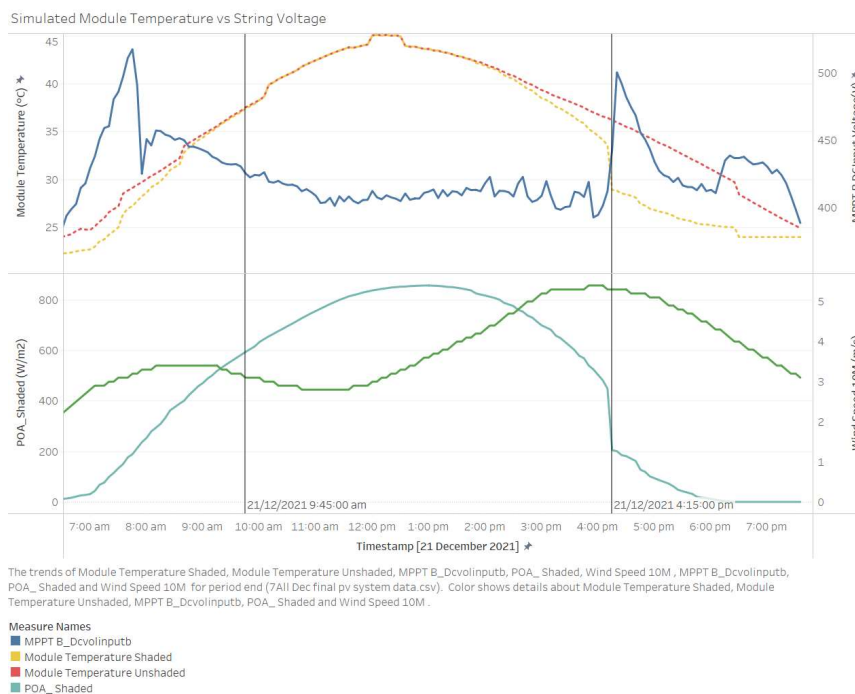


Figure 65 DC Voltage from String 7C vs Meteorological Data

On analyzing the graph in Figure 64, the voltage and current output from the string, at 07:55:00AM, the sudden ramp-up of DC current and voltage is observed due to the sun's position hitting the horizon to the PV String's location. However, by 04:10 PM, as the shading percentage of the

The graph in Figure 65 compares the Simulated Module Temperature against the DC voltage from the PV String from 07:00 AM. As the module's temperature increases with reduced windspeed, the effect is seen on the PV voltage. As the sun rises above the horizon, a sudden voltage drops. It's evident that the voltage decreases as the module temperature increases; at 04:15 PM, as the string reaches 100% shading, the drop in Shaded Plane of

Array Irradiance leads to a reduction in module temperature; it predominantly observed that the windspeed_10m gradually increases towards the evening, leading to faster cooling of the module, and a sharp increase in voltage.

The result and analysis of the above graphs show a connection and correlating patterns between the electrical and meteorological parameters of the Simulated model and the electrical parameters from the actual Inverter.

6. Discussion

This section provides an independent discussion of the study's outcomes. As the study aims to analyze the underperformance of PV due to shading on the DC Side through LIDAR, the primary component of this study involves modelling the LIDAR components to model the shading impacts on the PV String effectively. However, when comparing the simulated power (DC) and the actual inverter MPPT Power (DC) from the PV String, a minute deviation is observed in the plotted data. The graph in the figure 66-67 indicates that the simulation provides a closer value to the actual DC Power. It is observed that the error between the simulated and actual DC Power data is less when the power levels are less than 500W and 2700 W. The errors have been quantified through RMSE, MAE, MAPE, and nRMSE of 350.80W, 272.93W, 47.85%, and 0.13, respectively, as seen in the figure.68

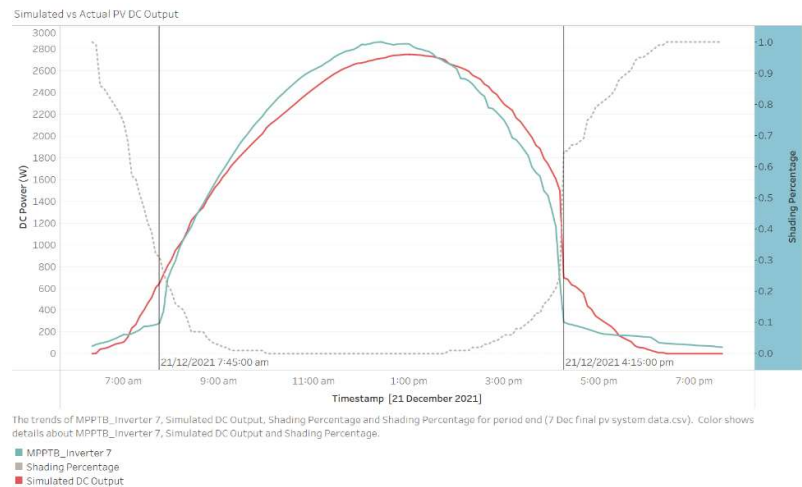


Figure 66 Inverter MPPT DC Power Input vs Simulated DC Output vs Shading Percentage

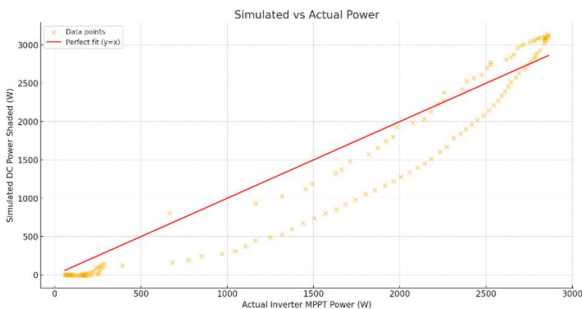


Figure 67 Simulated Shaded DC Power vs Actual DC Power from Inverter

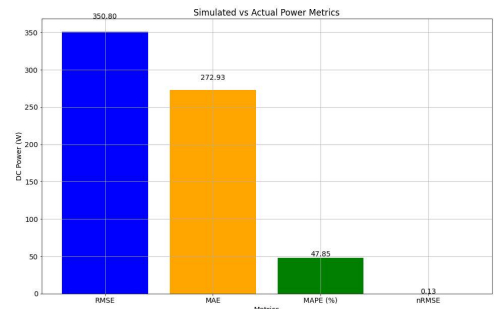


Figure 68 RMSE, MAE, MAPE, and nRMSE Metrics for shaded simulated vs actual DC Power Output

In due course of the study, the shadowing impacts are calculated from a String level; however, in real-time, the module-level study would further improve and reduce the error between the simulated and actual values in DC. This is because as shading occurs on a module level, the bypass diodes would turn up to shut down the portion of shaded cells in the module, causing sudden ripples of Voltage spikes when the shading on the string increases gradually post-02:00 PM, as seen in the figure. As a result of string level analysis at 04:15 PM, when the shading percentage reaches 65%, the actual inverter power is comparatively lower than predicted. The Sharp ramp rates of the shading factor / shading percentage are an effect of shading on the PV Panels caused by rooflines and facades.

The model used in determining the shadowing impacts on a given area would change based on the observed tilt angle. As seen in the figure, running the model on a flat roof area at the NIDA building provides well-defined shading boundaries; however, since the analyzed PV string is at an orientation of 45°, the estimation of the Shading factor would defer due to the angle of the roofline in close relation with the tower, as seen in Fig.

Further observing the study's outcomes, the Shadow Impact Analysis (a proprietary solution tool from ArcGIS) on 3D buildings provides a rough outlook on the areas of the roof to which shadow occurs from a 3D perspective. The proposed model to generate the shading profile of the PV String using the Hillshade Tool provides closer estimations of the shading factor, leading to realistic simulation data.

From the design perspective, the shadow impact analysis tool could be used to analyze the impact of shading caused by the facades of other buildings and the buildings to be observed; however, the hillshade analysis can estimate shading caused by the facades of buildings as well as the vegetation around the observed area, therefore providing closer estimations of shading due to temporal and permanent objects.

From the above discussion of the results, a correlation between the simulated system and the actual PV system has been established, and the effects of shading have been translated into the change in the output, voltage, and current of the PV String; it is evident that the estimation of the shadowing effects on a PV System is feasible through modelling LIDAR.

7. Conclusion and Future Directions

The main results of the study are concluded, and a few directions for future work are also provided.

7.1 Research Results

In Sections 1 and 2, the thesis introduces its organization, background, and fundamental research objectives and contributions. Section 3 identifies critical issues related to the performance drop in PV systems. It discusses the literature on quantifying performance losses, particularly due to shading, and provides a range of approaches, then narrows down the approach to using LIDAR to estimate shading.

In section 4, an approach is derived to estimate the impacts of shadow on the PV system. The proposed workflow starts by recognizing the required data types and sources to model the shadow of a simulated system. Some of the critical findings post-modelling were:

- A dual approach has been taken to model the shadows and identify the shaded PV String.
- Performing shadow impact analysis using the Development Impact Analysis Tool from ArcGIS helps estimate the shading on 3D structures and identify the shaded portion of the roof area. This information is helpful in determining the PV string that needs further study and demonstrates the reliability of the tool for future studies.
- The Proposed model utilizes Hillshade Analysis to generate a timestamped profile of the shaded region of the PV string across the day. It provides a measurement of the shading factor, leading to a closer estimation of the simulated PV Power in comparison to the actual DC PV Power from the string.
- The proposed approach in the study could be applied to a broader spectrum of urban rooflines with LIDAR data to establish the shading effects on the PV systems from a design, operational, and maintenance level.

7.2 Future Directions

Although the study addressed the challenges of shading and quantifying its impacts, some potential directions for future work remain.

- Deeper Analysis of the Shading Impact: The effect of shadowing on the PV String is computed on the string level; however, considering a cell-level/module-level analysis that includes the impact of bypass diodes would increase the accuracy of simulated data.
- Reliability of the Model: The model could be further implemented on various types of sites that include PV modules of multiple orientations installed on various other kinds of rooflines; other

sources of LIDAR data (airborne, drone, and satellite) would further assess the accuracy of the estimations.

- Further studies using time series LIDAR data as a source to assess the performance of the PV System and identify potential methodology to incorporate LIDAR into the operational and maintenance of the PV Plant.

References

- Abd Latif, Z., Zaki, N.A.M., Salleh, S.A., 2012. GIS-based estimation of rooftop solar photovoltaic potential using LiDAR. Presented at the 2012 IEEE 8th international colloquium on signal processing and its applications, IEEE, pp. 388–392.
- Al Siyabi, I., Al Mayasi, A., Al Shukaili, A., Khanna, S., 2021. Effect of soiling on solar photovoltaic performance under desert climatic conditions. *Energies* 14, 659.
- Alhmoud, L., 2023. Why Does the PV Solar Power Plant Operate Ineffectively? *Energies* 16, 4074. <https://doi.org/10.3390/en16104074>
- Aslam, A., Ahmed, Naseer, Qureshi, S.A., Assadi, M., Ahmed, Naveed, 2022. Advances in Solar PV Systems; A Comprehensive Review of PV Performance, Influencing Factors, and Mitigation Techniques. *Energies* 15, 7595. <https://doi.org/10.3390/en15207595>
- Bocullo, V., Martišauskas, L., Pupeikis, D., Gatautis, R., Venčaitis, R., Bakas, R., 2023. UAV Photogrammetry Application for Determining the Influence of Shading on Solar Photovoltaic Array Energy Efficiency. *Energies* 16. <https://doi.org/10.3390/en16031292>
- Boz, M.B., Calvert, K., Brownson, J.R.S., Boz, M.B., Calvert, K., Brownson, J.R.S., 2015. An automated model for rooftop PV systems assessment in ArcGIS using LIDAR. *AIMSE* 3, 401–420. <https://doi.org/10.3934/energy.2015.3.401>
- Brecl, K., Topič, M., 2011. Self-shading losses of fixed free-standing PV arrays. *Renewable Energy* 36, 3211–3216.
- Capdevila, H., Marola, A., Herrerías, M., 2013. High resolution shading modelling and performance simulation of sun-tracking photovoltaic systems. Presented at the AIP Conference Proceedings, American Institute of Physics, pp. 201–204.
- Dash, P., Gupta, N., 2015. Effect of temperature on power output from different commercially available photovoltaic modules. *International Journal of Engineering Research and Applications* 5, 148–151.
- El-Ashmawy, N., Shaker, A., 2014. Raster Vs. Point Cloud LiDAR Data Classification. *Int. Arch. Photogramm. Remote Sens. Spatial Inf. Sci.* XL–7, 79–83. <https://doi.org/10.5194/isprsarchives-XL-7-79-2014>
- F. Holmgren, W., W. Hansen, C., A. Mikofski, M., 2018. pvlib python: a python package for modelling solar energy systems. *JOSS* 3, 884. <https://doi.org/10.21105/joss.00884>

- Freitas, S., Brito, M., 2017. Validation of a facade PV potential model based on LiDAR data. Presented at the Proceedings of the 33rd EUPVSEC European PV Solar Energy Conference and Exhibition, Amsterdam, The Netherlands, pp. 25–29.
- García, M.A., Herrmann, W., Böhmer, W., Proisy, B., 2003. Thermal and electrical effects caused by outdoor hot-spot testing in associations of photovoltaic cells. *Progress in photovoltaics: research and applications* 11, 293–307.
- Gawley, D., McKenzie, P., 2022. Investigating the suitability of GIS and remotely-sensed datasets for photovoltaic modelling on building rooftops. *Energy and Buildings* 265, 112083.
- Gergelova, M.B., Labant, S., Kuzevic, S., Kuzevicova, Z., Pavolova, H., 2020. Identification of Roof Surfaces from LiDAR Cloud Points by GIS Tools: A Case Study of Lučenec, Slovakia. *Sustainability* 12, 6847. <https://doi.org/10.3390/su12176847>
- Goss, B., Cole, I., Betts, T., Gottschalg, R., 2014. Irradiance modelling for individual cells of shaded solar photovoltaic arrays. *Solar Energy* 110, 410–419.
- Govekar, P.D., Griffin, C., Beggs, H., 2022. Multi-Sensor Sea Surface Temperature Products from the Australian Bureau of Meteorology. *Remote Sensing* 14, 3785. <https://doi.org/10.3390/rs14153785>
- Hanifi, H., Khan, M.Z., Jaekel, B., Hagendorf, C., Schneider, J., Abdallah, A., Ilse, K., 2020. Optimum PV module interconnection layout and mounting orientation to reduce inhomogeneous soiling losses in desert environments. *Solar Energy* 203, 267–274.
- Herbei, M.V., Ciolac, V., Șmuleac, A., Nistor, E., Ciolac, L., 2010. Georeferencing of topographical maps using the software ARCGIS. *Research Journal of Agricultural Science* 42, 595–606.
- Jayaraj, P., Ramiya, A.M., 2018. 3D CITYGML BUILDING MODELLING FROM LIDAR POINT CLOUD DATA. *The International Archives of the Photogrammetry, Remote Sensing and Spatial Information Sciences XLII-5*, 175–180. <https://doi.org/10.5194/isprs-archives-XLII-5-175-2018>
- Jordan, D.C., Deline, C., Kurtz, S.R., Kimball, G.M., Anderson, M., 2017. Robust PV degradation methodology and application. *IEEE Journal of photovoltaics* 8, 525–531.
- Khanna, A., Mueller, T., Stangl, R.A., Hoex, B., Basu, P.K., Aberle, A.G., 2013. A fill factor loss analysis method for silicon wafer solar cells. *IEEE Journal of Photovoltaics* 3, 1170–1177.
- Killinger, S., Engerer, N., Müller, B., 2017. QCPV: A quality control algorithm for distributed photovoltaic array power output. *Solar Energy* 143, 120–131.
- Kim, J., Rabelo, M., Padi, S.P., Yousuf, H., Cho, E.-C., Yi, J., 2021. A review of the degradation of photovoltaic modules for life expectancy. *Energies* 14, 4278.

- Latif, Z.A., Zaki, N.A.M., Salleh, S.A., 2012. GIS-based estimation of rooftop solar photovoltaic potential using LiDAR, in: 2012 IEEE 8th International Colloquium on Signal Processing and Its Applications. Presented at the 2012 IEEE 8th International Colloquium on Signal Processing and its Applications, pp. 388–392. <https://doi.org/10.1109/CSPA.2012.6194755>
- Li, Y., Ding, D., Liu, C., Wang, C., 2016. A pixel-based approach to estimation of solar energy potential on building roofs. *Energy and Buildings* 129, 563–573.
- Li, Z., Zhang, Z., Davey, K., 2015. Estimating geographical PV potential using LiDAR data for buildings in downtown San Francisco. *Transactions in GIS* 19, 930–963.
- Liao, W., Heo, Y., Xu, S., 2019. Simplified vector-based model tailored for urban-scale prediction of solar irradiance. *Solar Energy* 183, 566–586.
- Lingfors, D., Bright, J.M., Engerer, N.A., Ahlberg, J., Killinger, S., Widén, J., 2017. Comparing the capability of low-and high-resolution LiDAR data with application to solar resource assessment, roof type classification and shading analysis. *Applied Energy* 205, 1216–1230.
- Lingfors, D., Killinger, S., Engerer, N.A., Widén, J., Bright, J.M., 2018. Identification of PV system shading using a LiDAR-based solar resource assessment model: An evaluation and cross-validation. *Solar Energy* 159, 157–172. <https://doi.org/10.1016/j.solener.2017.10.061>
- Liu, J., Matolak, D.W., 2018. Worst Month Tropospheric Attenuation Variability Analysis: ITU Model vs. Rain Gauge Data for Air-Satellite Links. 2018 11th Global Symposium on Millimeter Waves (GSMM) 1–5. <https://doi.org/10.1109/GSMM.2018.8439347>
- Lukač, N., Seme, S., Žlaus, D., Štumberger, G., Žalik, B., 2014. Buildings roofs photovoltaic potential assessment based on LiDAR (Light Detection And Ranging) data. *Energy* 66, 598–609.
- Lukač, N., Žalik, B., 2013. GPU-based roofs' solar potential estimation using LiDAR data. *Computers & Geosciences* 52, 34–41.
- Luo, W., Khoo, Y.S., Hacke, P., Naumann, V., Lausch, D., Harvey, S.P., Singh, J.P., Chai, J., Wang, Y., Aberle, A.G., 2017. Potential-induced degradation in photovoltaic modules: a critical review. *Energy & environmental science* 10, 43–68.
- Meyers, B., Mikofski, M., Anderson, M., 2016. A fast parameterized model for predicting PV system performance under partial shade conditions. Presented at the 2016 IEEE 43rd Photovoltaic Specialists Conference (PVSC), IEEE, pp. 3173–3178.
- Miranda, E., Fierro, J.F.G., Narváez, G., Giraldo, L.F., Bressan, M., 2021. Prediction of site-specific solar diffuse horizontal irradiance from two input variables in Colombia. *Heliyon* 7, e08602. <https://doi.org/10.1016/j.heliyon.2021.e08602>

- Munoz, M., Alonso-García, M.C., Vela, N., Chenlo, F., 2011. Early degradation of silicon PV modules and guaranty conditions. *Solar energy* 85, 2264–2274.
- Nassar, Y.F., Hafez, A.A., Alsadi, S.Y., 2020. Multi-Factorial Comparison for 24 Distinct Transposition Models for Inclined Surface Solar Irradiance Computation in the State of Palestine: A Case Study. *Front. Energy Res.* 7. <https://doi.org/10.3389/fenrg.2019.00163>
- Nguyen, H.T., Pearce, J.M., Harrap, R., Barber, G., 2012a. The application of LiDAR to assessment of rooftop solar photovoltaic deployment potential in a municipal district unit. *Sensors* 12, 4534–4558.
- Nguyen, H.T., Pearce, J.M., Harrap, R., Barber, G., 2012b. The application of LiDAR to assessment of rooftop solar photovoltaic deployment potential in a municipal district unit. *Sensors* 12, 4534–4558.
- Nordmann, T., Clavadetscher, L., Sark, W., Green, M., 2015. Analysis of Long-Term Performance of PV Systems.
- Pachauri, R.K., Kansal, I., Babu, T.S., Alhelou, H.H., 2021. Power losses reduction of solar PV systems under partial shading conditions using re-allocation of PV module-fixed electrical connections. *IEEE Access* 9, 94789–94812.
- Pavan, A.M., Mellit, A., De Pieri, D., 2011. The effect of soiling on energy production for large-scale photovoltaic plants. *Solar energy* 85, 1128–1136.
- Pham, M.-H., Phap, V.M., Trung, N.N., Son, T.T., Kien, D.T., Anh Tho, V.T., 2022. A Study on the Impact of Various Meteorological Data on the Design Performance of Rooftop Solar Power Projects in Vietnam: A Case Study of Electric Power University. *Energies* 15, 7149. <https://doi.org/10.3390/en15197149>
- Pillai, D.S., Blaabjerg, F., Rajasekar, N., 2019. A Comparative Evaluation of Advanced Fault Detection Approaches for PV Systems. *IEEE Journal of Photovoltaics* 9, 513–527. <https://doi.org/10.1109/JPHOTOV.2019.2892189>
- Radosevic, N., Liu, G.-J., Tapper, N., Zhu, X., Sun, Q.C., 2022. Solar Energy Modelling and Mapping for the Sustainable Campus at Monash University. *Frontiers in Sustainable Cities* 3, 745197.
- Rahman, M., Hasanuzzaman, M., Rahim, N.A., 2015. Effects of various parameters on PV-module power and efficiency. *Energy Conversion and Management* 103, 348–358.
- Reda, I., Andreas, A., 2008. Solar Position Algorithm for Solar Radiation Applications (Revised) (No. NREL/TP-560-34302, 15003974). <https://doi.org/10.2172/15003974>

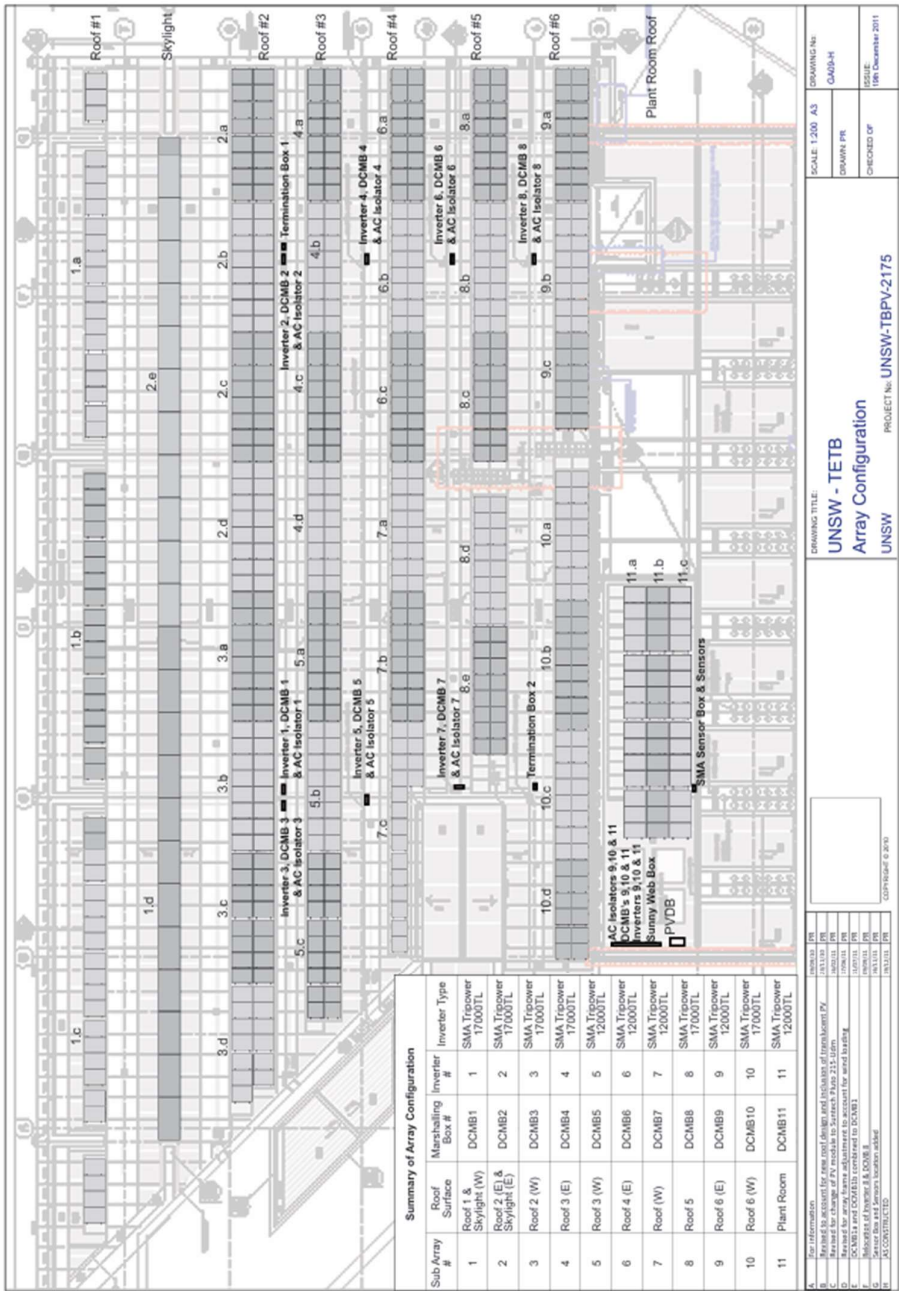
- Saiprakash, C., Mohapatra, A., Nayak, B., Ghatak, S.R., 2021. Analysis of partial shading effect on energy output of different solar PV array configurations. *Materials Today: Proceedings* 39, 1905–1909.
- Satpathy, P.R., Sharma, R., 2020. Reliability and losses investigation of photovoltaic power generators during partial shading. *Energy Conversion and Management* 223, 113480.
- Sayago, S., Ovando, G., Almorox, J., Bocco, M., 2020. Daily solar radiation from NASA-POWER product: assessing its accuracy considering atmospheric transparency. *International Journal of Remote Sensing* 41, 897–910. <https://doi.org/10.1080/01431161.2019.1650986>
- Schultz, A.J., 2012. The role of GIS in asset management: Integration at the Otay Water District. Presented at the Masters Abstracts International.
- Shaikh, R.A., Vowles, D.J., Allison, A., Abbott, D., 2023. Evaluation of Australia's Generation-Storage Requirements in a Fully Renewable Grid With Intermittent and Flexible Generation. *IEEE Access* 11, 64201–64218. <https://doi.org/10.1109/ACCESS.2023.3286037>
- Sharma, D.K., Purohit, G., 2014. Analysis of the effect of fill factor on the efficiency of solar PV system for improved design of MPPT. Presented at the 6th world conference on photo voltaic energy conversion.
- Skomedal, Å.F., Aarseth, B.L., Haug, H., Selj, J., Marstein, E.S., 2020. How much power is lost in a hot-spot? A case study quantifying the effect of thermal anomalies in two utility scale PV power plants. *Solar Energy* 211, 1255–1262.
- Skomedal, A.F., Ogaard, M.B., Haug, H., Marstein, E.S., 2021. Robust and Fast Detection of Small Power Losses in Large-Scale PV Systems. *IEEE J. Photovoltaics* 1–8. <https://doi.org/10.1109/JPHOTOV.2021.3060732>
- Solcast: Validation of a satellite-derived solar irradiance dataset, 2019. . *Solar Energy* 189, 435–449. <https://doi.org/10.1016/j.solener.2019.07.086>
- Tian, B., n.d. A LiDAR DSM based geometry modelling method to improve solar irradiance simulation and PV yield prediction in urban environments.
- Tröster, E., Schmidt, J.-D., 2012. Evaluating the impact of PV module orientation on grid operation. Presented at the Proceedings of the 2nd International Workshop on Integration of Solar Power into Power Systems, Lisbon, Portugal.
- Vega-Garita, V., Alpizar-Gutierrez, V., Alpizar-Castillo, J., 2023. A practical method for considering shading on photovoltaics systems energy yield. *Energy Conversion and Management: X* 20, 100412. <https://doi.org/10.1016/j.ecmx.2023.100412>

- Xie, Y., Xie, B., Wang, Z., Gupta, R.K., Baz, M., AlZain, M.A., Masud, M., 2022. Geological resource Planning and environmental Impact assessments based on GIS. *Sustainability* 14, 906.
- Yang, D., Bright, J.M., 2020. Worldwide validation of 8 satellite-derived and reanalysis solar radiation products: A preliminary evaluation and overall metrics for hourly data over 27 years. *Solar Energy* 210, 3–19. <https://doi.org/10.1016/j.solener.2020.04.016>
- Yousuf, M.U., Siddiqui, M., 2018. Solar energy potential estimation by calculating sun illumination hours and sky view factor on building rooftops using digital elevation model. *Journal of Renewable and Sustainable Energy* 10.
- Zhang, Y., Su, J., Zhang, C., Lang, Z., Yang, M., Gu, T., 2021. Performance estimation of photovoltaic module under partial shading based on explicit analytical model. *Solar Energy* 224, 327–340.
- Zhao, C., Xiao, J., Yu, Y., Jaubert, J.-N., 2021. Accurate shading factor and mismatch loss analysis of bifacial HSAT systems through ray-tracing modelling. *Solar Energy Advances* 1, 100004. <https://doi.org/10.1016/j.seja.2021.100004>
- Zhong, D., Haiyan, Y., 2023. Research on Power Grid Data Asset Management Based on Big Data BI Analysis—The Role of Renewable Energy Technologies. *Strategic Planning for Energy and the Environment* 585–614.
- Zorrilla-Casanova, J., Piliouline, M., Carretero, J., Bernaola-Galván, P., Carpena, P., Mora-López, L., Sidrach-de-Cardona, M., 2013. Losses produced by soiling in the incoming radiation to photovoltaic modules. *Progress in photovoltaics: Research and applications* 21, 790–796.
- Zsiboracs, H., Zentko, L., Pinter, G., Vincze, A., Baranyai, N.H., 2021. Assessing shading losses of photovoltaic power plants based on string data. *Energy Reports* 7, 3400–3409.

Appendix A

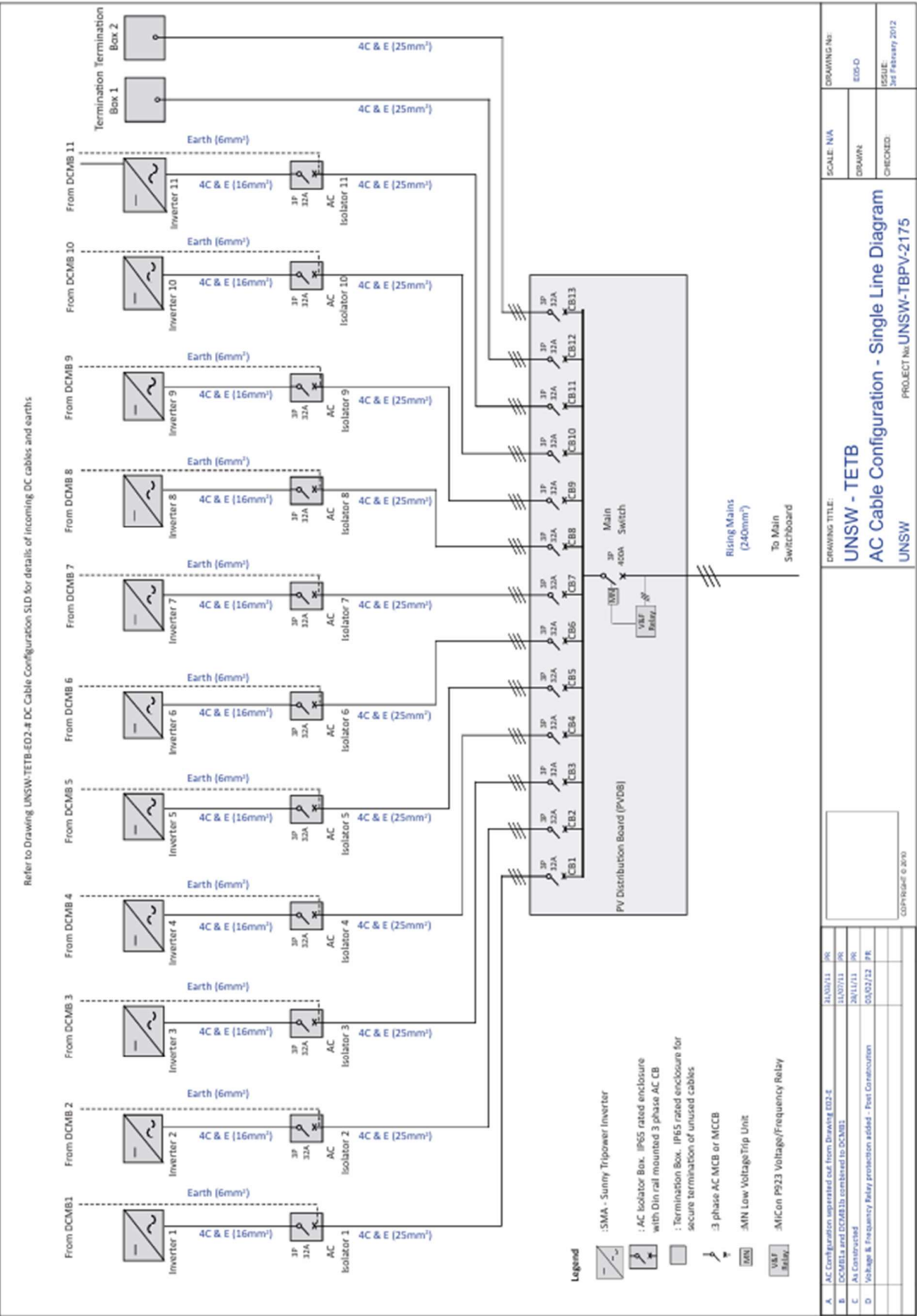
Datasheets and PV Schematics

1. PV Schematics Page 1



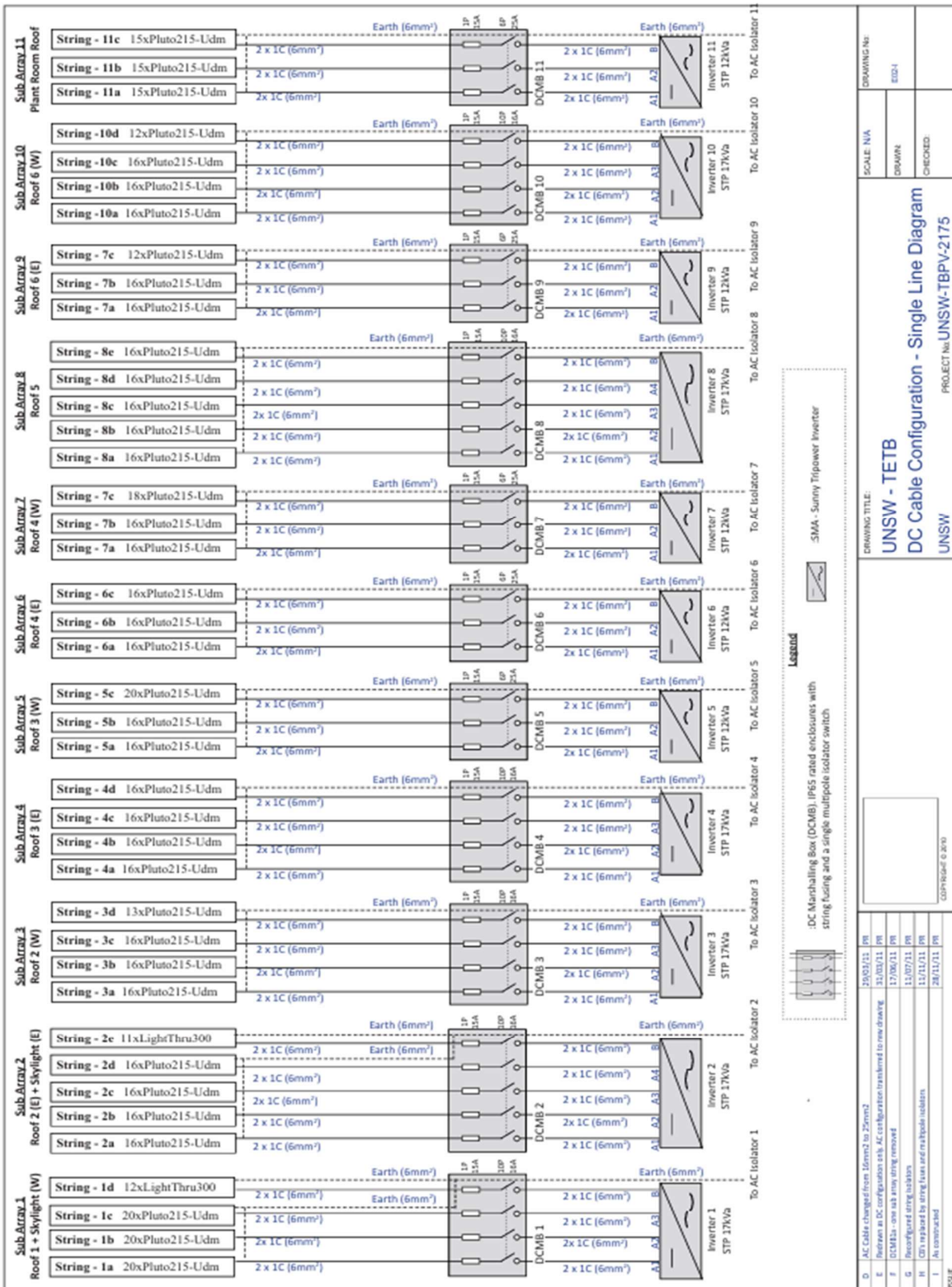
The underperformance of PV Systems on the DC Side
Understanding shading Effects in PV Systems using LIDAR

2. Single Line Diagram of TETB




The underperformance of PV Systems on the DC Side
Understanding shading Effects in PV Systems using LIDAR

3. String Configuration of TETB PV System




6. PV Data Request for TETB PV System from DARTH




Download


Rahul Ashwin Mahendhran

Select Parameters to Download .CSV File


 (Not selecting the below filters might download the complete database)

 Choose a Data Type :


photovoltaics

 Choose a Building:

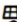
PV-TETB

 From Time Stamp:

20/06/2020 12:00:00 AM

 To Time Stamp:


24/06/2024 12:00:00 AM

 Choose a Device Serial Number:

Download .CSV File

Reset


7. Meteorological Data Request from Solcast




Historical and TMY
2007 to 7 days

Live and Forecast
7 days to 16 days

Rahul Ashwin Mahendhran



Create a New Time Series Request



Create a New TMY Request

Batch Requests

Showing 1-9 of your 9 requests

Batch Id

Search for a request

Q

Refresh

Request Date	Batch Id	Request Type	Detail	Status	Actions
2024-08-07 05:21	e426364d...	Historic Radiation and Weather	1 locations	Ready	Download
2024-08-06 22:03	d99a44ea...	Historic Radiation and Weather	1 locations	Ready	Download
2024-08-06 00:47	3c9e7fce...	Historic Radiation and Weather	1 locations	Ready	Download
2024-08-06 00:45	f7e1acfe...	Historic Radiation and Weather	1 locations	Ready	Download
2024-08-02 00:52	4d3c9c2d...	Historic Radiation and Weather	1 locations	Ready	Download

Appendix B

1. Calculate POA vs GHI

```
# -*- coding: utf-8 -*-
"""
Created on Wed Jun 12 06:29:48 2024

@author: rahul
"""

import pandas as pd
import matplotlib.pyplot as plt
import pvlib
from pvlib.location import Location
import matplotlib.dates as mdates # Import mdates for date
formatting

weather_data = pd.read_csv('E:/Filter/2021-12-
21_weather_data_filter.csv')

weather_data['period_end'] =
pd.to_datetime(weather_data['period_end'])
weather_data.set_index('period_end', inplace=True)

# location and system parameters
location = Location(latitude=-33.8688, longitude=151.2093,
tz='Australia/Sydney')
tilt = 45
azimuth = 12
surface_tilt = tilt
surface_azimuth = azimuth

# Calculate solar position
solar_position = location.get_solarposition(weather_data.index)

# Calculate extra terrestrial radiation
extra_radiation =
pvlib.irradiance.get_extra_radiation(weather_data.index)

# Calculate AOI (angle of incidence)
aoi = pvlib.irradiance.aoi(surface_tilt, surface_azimuth,
solar_position['apparent_zenith'],
solar_position['azimuth'])

# Calc POA sky diffuse
poa_sky_diffuse = pvlib.irradiance.haydavies(surface_tilt,
surface_azimuth,
weather_data['ghi'],
weather_data['dhi'], weather_data['dni'],
solar_position['apparent_zenith'], solar_position['azimuth'])

# Calc POA ground diffuse
poa_ground_diffuse =
pvlib.irradiance.get_ground_diffuse(surface_tilt,
weather_data['ghi'])

# Calc POA total
poa_total = pvlib.irradiance.poa_components(aoi,
weather_data['dni'], poa_sky_diffuse, poa_ground_diffuse)

# Add POA to the weather data
weather_data['poa'] = poa_total['poa_global']
```

```
plt.rcParams.update({'font.size': 14})

# Plot GHI vs POA
plt.figure(figsize=(10, 6))
plt.plot(weather_data.index, weather_data['ghi'], label='GHI')
plt.plot(weather_data.index, weather_data['poa'], label='POA')

plt.gca().xaxis.set_major_formatter(mdates.DateFormatter('%H:%M'))

plt.xlabel('Time')
plt.ylabel('Irradiance (W/m^2)')
plt.title('GHI vs POA')
plt.legend()
plt.grid(True)
plt.tight_layout()
plt.show()
```

2. Solar Azimuth and Elevation Calculator

```
# -*- coding: utf-8 -*-
"""
Created on Mon Jun  3 16:26:56 2024

@author: rahul
"""

import pvlib
from datetime import datetime, timedelta
import pytz
import pandas as pd
import matplotlib.pyplot as plt

def calc_solar_positions(latitude, longitude, timezone, date):
    # start and end times
    start_time = datetime(date.year, date.month, date.day, 5, 0, 0)
    end_time = datetime(date.year, date.month, date.day, 20, 0, 0)

    # Localize times to the specified timezone
    localized_start_time = pytz.timezone(timezone).localize(start_time)
    localized_end_time = pytz.timezone(timezone).localize(end_time)

    # Generate a list of times at 30-minute intervals
    times = pd.date_range(localized_start_time, localized_end_time,
                           freq='15min')

    # Calc solar positions for all times
    solar_positions = pvlib.solarposition.get_solarposition(times, latitude,
                                                             longitude)

    return times, solar_positions

# location (latitude, longitude, timezone)
latitude = -33.91769
longitude = 151.2270
timezone = 'Australia/Sydney'

# date
date = datetime(2021, 12, 21)

# Calc solar positions
```

```
times, solar_positions = calc_solar_positions(latitude, longitude, timezone,
date)

# DataFrame with datetime, time, azimuth, and elevation
data = {
    'Datetime': times,
    'Time': times.strftime('%d/%m/%Y %I:%M:%S %p'),
    'Filer': times.strftime('%H %M %S'),
    'Azimuth': solar_positions['azimuth'].values,
    'Elevation': solar_positions['elevation'].values
}

solar_positions_df = pd.DataFrame(data)

# Filter the DataFrame to keep only rows where the elevation is greater than 0
solar_positions_df = solar_positions_df[solar_positions_df['Elevation'] > 0]

# Generate the dynamic CSV file path
csv_file_path =
rf'H:\TETB\model\solarpos\{date.strftime("%Y_%m_%d")}_15m_solar1_positions.csv'
solar_positions_df.to_csv(csv_file_path, index=False)

print(f"Solar positions have been saved to '{csv_file_path}'")

# Plot Azimuth and Elevation as smooth curves
fig, ax1 = plt.subplots(figsize=(10, 6))
# Add title
plt.title(f"Azimuth and Elevation on {date.strftime('%d/%m/%Y')}")

# Plot Azimuth on the primary axis using datetime for x-axis
ax1.plot(solar_positions_df['Datetime'], solar_positions_df['Azimuth'],
color='tab:blue', label='Azimuth', linestyle='-', linewidth=2)
ax1.set_xlabel('Time mm-dd (hh)')
ax1.set_ylabel('Azimuth (degrees)', color='tab:blue')
ax1.tick_params(axis='y', labelcolor='tab:blue')

# Enable gridlines for primary axis
ax1.grid(True)

# secondary axis for Elevation
ax2 = ax1.twinx()
ax2.plot(solar_positions_df['Datetime'], solar_positions_df['Elevation'],
color='tab:red', label='Elevation', linestyle='-', linewidth=2)
ax2.set_ylabel('Elevation (degrees)', color='tab:red')
ax2.tick_params(axis='y', labelcolor='tab:red')

ax1.xaxis.set_major_formatter(mdates.DateFormatter('%H'))
ax1.xaxis.set_major_locator(mdates.HourLocator(interval=1)) # Set major ticks
at every hour

# Rotate x-ticks for better readability
plt.xticks(rotation=0)

# Adjust layout to prevent overlapping
plt.tight_layout()
plt.show()
```

3. Modelling PV System with Weather and Shading Profile Data

```
# -*- coding: utf-8 -*-
"""
```

The underperformance of PV Systems on the DC Side
Understanding shading Effects in PV Systems using LIDAR

```
Created on Fri Jul 26 12:14:35 2024

@author: rahul
"""

import pandas as pd
import pvlib
import matplotlib.pyplot as plt
from pvlib.location import Location
import matplotlib.dates as mdates

# Load the data from the provided files
weather_data = pd.read_csv('E://Filter/2021-12-21_weather_data_filter.csv')
shading_data = pd.read_csv('E://Filter/Consolidated_Dec7_Data.csv')

# Ensure the weather data has a proper timestamp index
weather_data['period_end'] = pd.to_datetime(weather_data['period_end'],
dayfirst=True)

weather_data['period_end'] =
weather_data['period_end'].dt.tz_localize('UTC').dt.tz_convert(None)
shading_data['timestamp'] = pd.to_datetime(shading_data['timestamp'])

# Clean up the shading_percentage column
shading_data['shading_percentage'] =
shading_data['shading_percentage'].str.rstrip('%').astype('float') / 100.0

# Set index to timestamps
weather_data.set_index('period_end', inplace=True)
shading_data.set_index('timestamp', inplace=True)

# Merge the weather data with the shading data
combined_data = pd.merge(weather_data, shading_data, left_index=True,
right_index=True, how='inner')

# Filter out data points with low irradiance
irradiance_threshold = 50 # Irradiance threshold in W/m²
combined_data = combined_data[combined_data['ghi'] > irradiance_threshold]

location = Location(latitude=-33.8688, longitude=151.2093, tz='Australia/Sydney')
tilt = 50
azimuth = 10
surface_tilt = tilt
surface_azimuth = azimuth

# Retrieve module and inverter parameters
cec_modules = pvlib.pvsystem.retrieve_sam('cecmmod')
pv_module = 'Suntech_Power_PLUTO215_Udm'
module_parameters = cec_modules[pv_module]

cec_inverters = pvlib.pvsystem.retrieve_sam('cecinverter')
inverter = 'SMA_America_STP12000TL_US_10_480V_'
inverter_parameters = cec_inverters[inverter]

# Solar POA and Insolation Estimation

# Calc solar position
solar_position = location.get_solarposition(combined_data.index)

# Calc AOI (angle of incidence)
aoi = pvlib.irradiance.aoi(surface_tilt, surface_azimuth,
solar_position['apparent_zenith'],
solar_position['azimuth'])
```

The underperformance of PV Systems on the DC Side
Understanding shading Effects in PV Systems using LIDAR

```
# Calc POA sky diffuse
poa_sky_diffuse = pvlib.irradiance.haydavies(surface_tilt, surface_azimuth,
                                              combined_data['ghi'],
                                              combined_data['dhi'], combined_data['dni'],
                                              solar_position['apparent_zenith'],
                                              solar_position['azimuth'])

# Calc POA ground diffuse
poa_ground_diffuse = pvlib.irradiance.get_ground_diffuse(surface_tilt,
                                                          combined_data['ghi'])

# Calc POA total
poa_total = pvlib.irradiance.poa_components(aoi, combined_data['dni'],
                                             poa_sky_diffuse, poa_ground_diffuse)

# Add POA to the combined data
combined_data['poa_unshaded'] = poa_total['poa_global']

# Calc the POA irradiance for the shaded condition
combined_data['poa_shaded'] = combined_data['poa_unshaded'] * (1 -
                                                                combined_data['shading_percentage'])

# Plot the POA irradiance and DC power output
plt.figure(figsize=(14, 8))

plt.subplot(1, 1, 1)
plt.plot(combined_data.index, combined_data['poa_unshaded'], label='POA Unshaded')
plt.plot(combined_data.index, combined_data['poa_shaded'], label='POA Shaded')
plt.xlabel('Time')
plt.ylabel('POA Irradiance (W/m^2)')
plt.title('POA Irradiance (Shaded vs. Unshaded)')
plt.legend()

# Temperature Parameters
temperature_model_params =
pvlib.temperature.TEMPERATURE_MODEL_PARAMETERS['sapm']['open_rack_glass_polymer']

combined_data['temp_cell_unshaded'] = pvlib.temperature.sapm_module(
    poa_global=combined_data['poa_unshaded'],
    temp_air=combined_data['air_temp'],
    wind_speed=combined_data['wind_speed_10m'],
    a=-3.56,
    b=-0.075
)

# Calc DC power output using the pvsyst_dc model
combined_data['dc_power_unshaded'] = pvlib.pvsystem.pvwatts_dc(
    g_poa_effective=combined_data['poa_unshaded'],
    temp_cell=combined_data['temp_cell_unshaded'],
    pdc0=module_parameters['STC']*16,
    gamma_pdc=-0.0038
)

combined_data['temp_cell_shaded'] = pvlib.temperature.sapm_module(
    poa_global=combined_data['poa_shaded'],
    temp_air=combined_data['air_temp'],
    wind_speed=combined_data['wind_speed_10m'],
    a=-3.56,
    b=-0.075
)

combined_data['dc_power_shaded'] = pvlib.pvsystem.pvwatts_dc(
    g_poa_effective=combined_data['poa_shaded'],
```


The underperformance of PV Systems on the DC Side
Understanding shading Effects in PV Systems using LIDAR

```
temp_cell=combined_data['temp_cell_shaded'],
pdc0=module_parameters['STC']*16,
gamma_pdc=-0.0038

)

plt.rcParams.update({'font.size': 14})
plt.gca().xaxis.set_major_locator(mdates.HourLocator(interval=2))
plt.gca().xaxis.set_major_formatter(mdates.DateFormatter('%H:%M'))

# Plot the POA irradiance and DC power output side by side
fig, (ax1, ax2) = plt.subplots(1, 2, figsize=(16, 8))

# POA Irradiance
ax1.plot(combined_data.index, combined_data['poa_unshaded'], label='POA Unshaded')
ax1.plot(combined_data.index, combined_data['poa_shaded'], label='POA Shaded')
ax1.set_xlabel('Time')
ax1.set_ylabel('POA Irradiance (W/m^2)')
ax1.set_title('POA Irradiance (Shaded vs. Unshaded)')
ax1.legend()
ax1.xaxis.set_major_locator(mdates.HourLocator(interval=2))
ax1.xaxis.set_major_formatter(mdates.DateFormatter('%H:%M'))
ax1.grid(True) # Add gridlines

# DC Power Output
ax2.plot(combined_data.index, combined_data['dc_power_unshaded'], label='DC Power Unshaded')
ax2.plot(combined_data.index, combined_data['dc_power_shaded'], label='DC Power Shaded')
ax2.set_xlabel('Time')
ax2.set_ylabel('DC Power Output (W)')
ax2.set_title('DC Power Output (Shaded vs. Unshaded)')
ax2.legend()
ax2.xaxis.set_major_locator(mdates.HourLocator(interval=2))
ax2.xaxis.set_major_formatter(mdates.DateFormatter('%H:%M'))
ax2.grid(True)

plt.tight_layout()
plt.show()
```

4. Consolidator Code to process 174.csv

```
import pandas as pd
import os
from datetime import datetime

fixed_date = "21/12/2021"

# Folder path where files are stored
folder_path =
"H:\TETB\MyProject\GIS_data\June\9A_ACTUAL_MAIN\Zonal"
file_names = [f for f in os.listdir(folder_path) if
f.startswith('Zonal_PV3_Tetb_Str_Dec_Suns') and
f.endswith('.csv')]

reference_file_path = os.path.join(folder_path, "E://Tester.csv")
reference_data = pd.read_csv(reference_file_path)

consolidated_data = pd.DataFrame(columns=reference_data.columns)
```

```
# Process each file
for file_name in file_names:
    file_path = os.path.join(folder_path, file_name)

    # Extract time from the file name
    time_str = file_name.split('_')[-3:]
    time_str = ":".join(time_str).replace('.csv', '')
    datetime_str = f"{fixed_date} {time_str}"

    timestamp = datetime.strptime(datetime_str, '%d/%m/%Y
%H:%M:%S')

    data = pd.read_csv(file_path, usecols=[1, 2], header=None,
names=['Label', 'Count'])

    row = {'Timestamp': timestamp}
    for label, count in zip(data['Label'], data['Count']):
        row[str(label)] = count

    consolidated_data = pd.concat([consolidated_data,
pd.DataFrame([row])], ignore_index=True)

# Fill NaN with 0 (if any label is missing in a file)
consolidated_data = consolidated_data.fillna(0)

# Ensure all columns from the reference are present
for col in reference_data.columns:
    if col not in consolidated_data.columns:
        consolidated_data[col] = 0

# Reorder columns based on the reference file
consolidated_data = consolidated_data[reference_data.columns]

# Ensure 'Timestamp' is the first column
if 'Timestamp' in consolidated_data.columns:
    cols = ['Timestamp'] + [col for col in consolidated_data if
col != 'Timestamp']
    consolidated_data = consolidated_data[cols]

# Save the consolidated data to a CSV file
output_path = os.path.join(folder_path,
"E://Consolidated_june9A_Data.csv")
consolidated_data.to_csv(output_path, index=False)

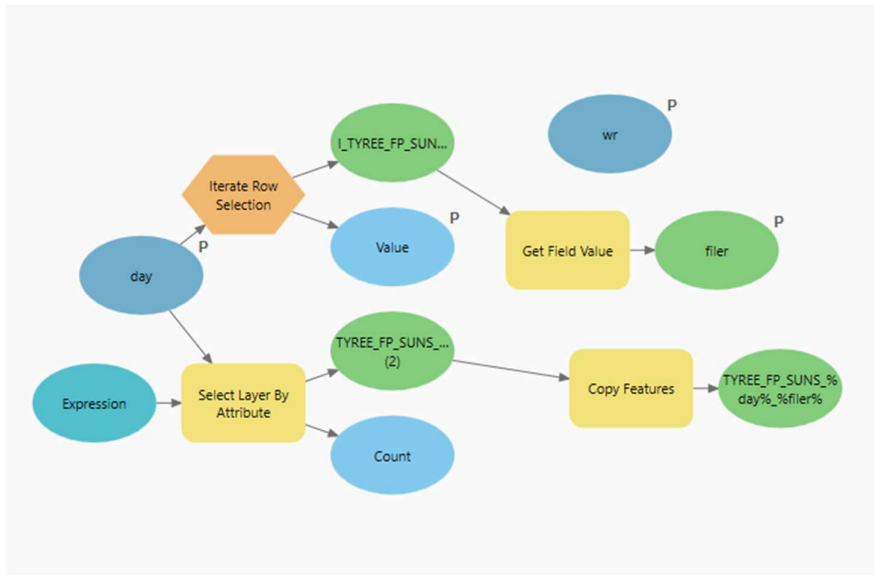
output_path
```

5. ModelBuilder for Shadow Impact Analysis

Modelbuilder 1

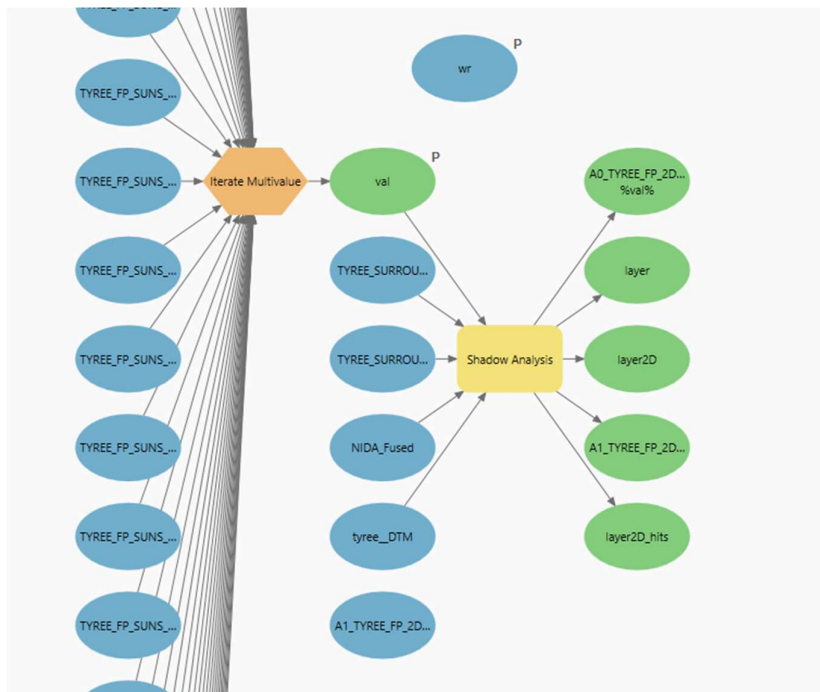
The underperformance of PV Systems on the DC Side

Understanding shading Effects in PV Systems using LIDAR



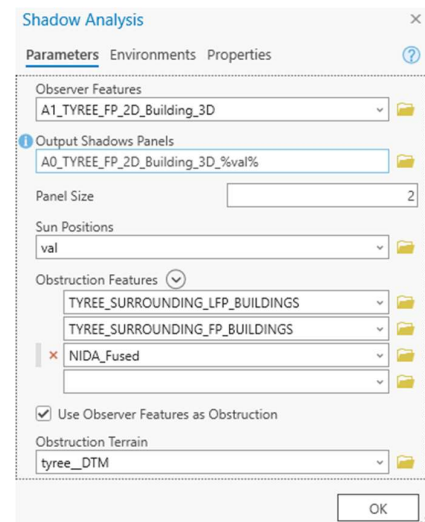
Inputs the Sun's Positions for the day as a Feature class and splits it into individual feature classes by OBJECT_ID to generate a singular feature class containing the Date, Time, Azimuth, and Elevation data.

ModelBuilder 2



Surrounding Buildings, and TETB itself. It then outputs shadow panel layers with a panel size 2x2m.

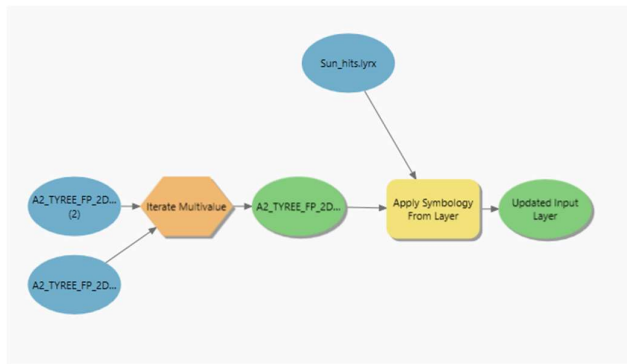
It inputs the individual feature class generated for ModelBuilder 1. It generates a shadow panel, taking observer features as the 3D TETB Multipatch and obstruction features as NIDA, TYREE



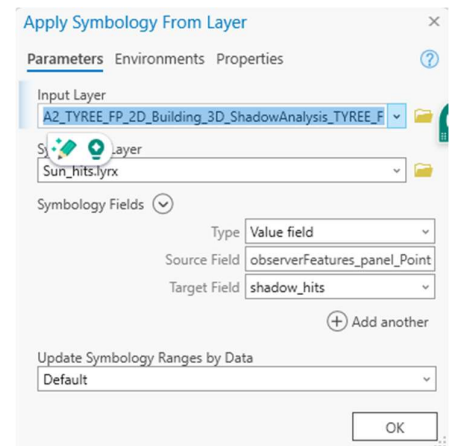
The underperformance of PV Systems on the DC Side

Understanding shading Effects in PV Systems using LIDAR

Model Builder 3

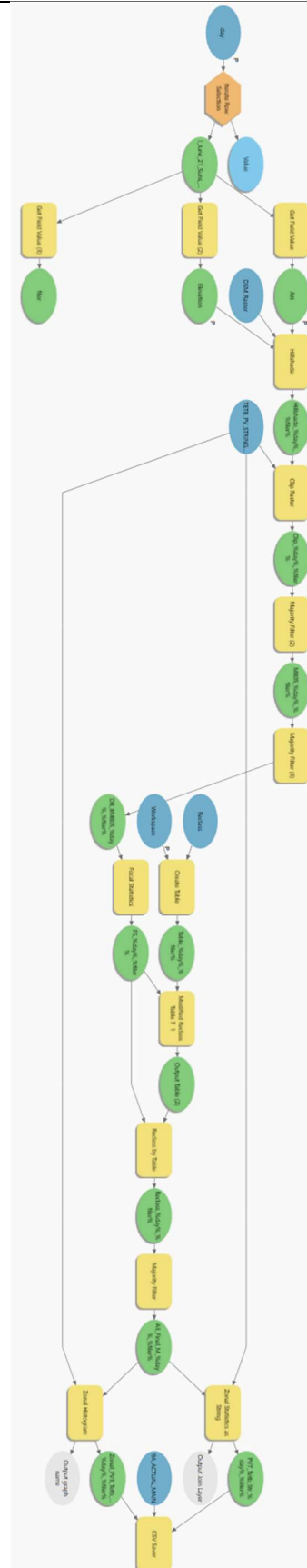


The output from ModelBuilder 2 is sent to ModelBuilder 3 to set the symbology of the shadow panels.



6. PV String Shading Profile Model

- PV String Analyser Model Inputs the Solar Azimuth and Elevation .csv from Appendix B.2
- Performs Hill Shade Analysis and models shadow
- Clips the raster based on the chosen PV String of study (String 7C Polygon)
- Performs 2x Majority Filter to populate shadows with zero pixels.
- After 2x Majority Filter, the raster is sent to perform Focal Statistics to smoothen sharp pixels to reduce noise.
- A Reclassification table is formed based on pyscript Appendix B.7 (2nd Standard Deviation by identifying the upper and lower limit of the processed raster) ,
- The Smoothened raster now gets reclassified based on the intervals generated in the reclassified table.
- A majority filter is put through to populate the shadowing pixels.
- Zonal Statistics and Histogram is performed on the final raster to get statistics of pixels within the area of the string.



7. Reclassifier Table Script (Arcpy)

```
import arcpy

def create_intervals_for_raster(raster_path, table_path):
    try:
        # Calculate raster properties
        min_val =
float(arcpy.GetRasterProperties_management(raster_path,
"MINIMUM").getOutput(0))
        max_val =
float(arcpy.GetRasterProperties_management(raster_path,
"MAXIMUM").getOutput(0))
        mean =
float(arcpy.GetRasterProperties_management(raster_path,
"MEAN").getOutput(0))
        std_dev =
float(arcpy.GetRasterProperties_management(raster_path,
"STD").getOutput(0))

        arcpy.AddMessage(f"Raster properties: min={min_val},
max={max_val}, mean={mean}, std_dev={std_dev}")

        intervals = [
            {"Interval": 2, "MinValue": max(min_val, mean - 2 *
std_dev), "MaxValue": max(min_val, mean - std_dev)},
            {"Interval": 3, "MinValue": max(min_val, mean -
std_dev), "MaxValue": max(min_val, mean - 0.5 * std_dev)},
            {"Interval": 4, "MinValue": max(min_val, mean - 0.5 *
std_dev), "MaxValue": min(max_val, mean + 0.5 * std_dev)},
            {"Interval": 5, "MinValue": min(max_val, mean + 0.5 *
std_dev), "MaxValue": min(max_val, mean + std_dev)},
            {"Interval": 6, "MinValue": min(max_val, mean +
std_dev), "MaxValue": min(max_val, mean + 2 * std_dev)},
            {"Interval": 7, "MinValue": min(max_val, mean + 2 *
std_dev), "MaxValue": max_val}
        ]

        # Explicitly handle 0 values shading
        zero_interval = {"Interval": 1, "MinValue": 0, "MaxValue":
0}

        arcpy.AddMessage(f"Generated intervals: {[zero_interval] +
intervals}")

        # Check if the table already exists
        if not arcpy.Exists(table_path):
            arcpy.AddError(f"The table does not exist:
{table_path}")
            return

        arcpy.AddMessage(f"Table exists: {table_path}")

        # Insert rows into the existing table
        with arcpy.da.InsertCursor(table_path, ["RasterName",
"Interval", "MinValue", "MaxValue"]) as cursor:
            cursor.insertRow((raster_path,
zero_interval["Interval"], zero_interval["MinValue"],
zero_interval["MaxValue"]))
            arcpy.AddMessage(f"Inserted row: {zero_interval}")
            for interval in intervals:
                cursor.insertRow((raster_path,
interval["Interval"], interval["MinValue"], interval["MaxValue"]))
```

```
        arcpy.AddMessage(f"Inserted row: {interval}")

    arcpy.AddMessage(f"Intervals successfully added to table:
{table_path}")
    return table_path

    except arcpy.ExecuteError as e:
        arcpy.AddError(f"Geoprocessing error: {e}")
        raise
    except Exception as e:
        arcpy.AddError(f"General error: {e}")
        raise

# Example usage
if __name__ == "__main__":
    raster_path = arcpy.GetParameterAsText(0) # Input raster
    table_path = arcpy.GetParameterAsText(1) # Pre-generated
table path

    # Create intervals and add them to the pre-generated table
    output_table = create_intervals_for_raster(raster_path,
table_path)

    # Set the output parameter to the created table
    arcpy.SetParameterAsText(2, output_table)
```